The Thesis Committee for Trevor Butler Yates
Certifies that this is the approved version of the following thesis:

Hydraulic Performance and Stability of Geosynthetic Landfill Cover Systems with Constrained Drainage at the Outlet

APPROVED BY
SUPERVISING COMMITTEE:

Supervisor: _____
Robert Gilbert

Co-Supervisor: _____
Jorge Zornberg

Reader: _____
Chadi El Mohtar

Hydraulic Performance and Stability of Geosynthetic Landfill Cover Systems with Constrained Drainage at the Outlet

by

Trevor Butler Yates, BSE

Thesis

Presented to the Faculty of the Graduate School of

The University of Texas at Austin

in Partial Fulfillment

of the Requirements

for the Degree of

Master of Science in Engineering

The University of Texas at Austin

August 2011

Dedication

For my wife Caitlin, my newborn son Bo, and my mother Martha.

Acknowledgements

I would like to thank my advisor, Dr. Bob Gilbert, for his guidance and encouragement throughout this research project. I would also like to thank my co-advisor, Dr. Jorge Zornberg, for making research engaging and for challenging me to broaden the scope of this research project.

I would like to thank Sam Allen and John Allen of Texas Research International for introducing a compelling topic and for facilitating every part of this thesis.

I would like to thank my officemates Julio Zambrano, Jeff Kuhn, Michael Plaisted, and Hossein Roodi, and my classmates Mary Goff, Katelyn McCarthy, Trent Ellis, and Danny Bosley for making my time at UT so productive and enjoyable.

Abstract

Hydraulic Performance and Stability of Geosynthetic Landfill Cover Systems with Constrained Drainage at the Outlet

Trevor Butler Yates, MSE

The University of Texas at Austin, 2011

Supervisor: Robert Gilbert

Co-Supervisor: Jorge Zornberg

Sliding failures of landfill cover systems are common, and the slip surface is often at the interface between a geosynthetic drainage layer and an underlying textured geomembrane. In an effort to understand the sliding failures, the objectives of this research project are to summarize current regulation and practice in landfill cover design, use experimental methods to characterize the behavior of geosynthetic landfill materials in cover systems approaching failure, and develop models to evaluate the hydraulic performance and stability of landfill cover systems.

Inclined plane tests were conducted to explore the behavior of a geosynthetic drainage material/textured geomembrane interface. The interface had effective normal stress dependent strain softening behavior, with more strain softening measured at higher effective normal stresses.

A numerical model for confined flow in a drainage layer with a constrained outlet was developed. The model was used to evaluate how water fills and empties from a geosynthetic drainage layer for a variety of inflow conditions and constraints to flow at the outlet. The model was used to demonstrate that a drainage layer that effectively conveys water out of a cover system with a free flowing drainage outlet quickly fills with water when the outlet has a modest constraint to flow.

An iterative, numerical model was developed to calculate stability solutions for landfill cover slopes that satisfy force equilibrium and strain compatibility while accounting for effective normal stress dependent strain softening and various pore water pressure conditions. Stability solutions reveal that depending on the water pressure in the drainage layer, the geosynthetic drainage material may experience tension at many points along the slope.

It is crucial for the stability of the landfill cover system to maintain free-flowing conditions at the drainage layer outlet. A modest constraint to flow at the outlet has a significant adverse effect on the ability of the landfill cover drainage layer to convey water out of the system, which can lead to instability. The drainage layer outlet should be designed to ensure free flow of water out of the drainage layer.

Table of Contents

List of Tables

List of Figures

CHAPTER 1: INTRODUCTION

1.1 PROBLEM STATEMENT

Landfills receive much of the municipal solid waste generated in the United States and in many other countries around the world. In the US, landfill permitting, design, construction, operation, and closure are regulated by the US Environmental Protection Agency and state environmental regulators. The design of landfill liner and cover systems is dictated by prescriptive guidelines specifying natural and geosynthetic materials for construction. The purpose of landfill final cover systems is to minimize leachate generation by preventing infiltrating water from entering the waste.

Sliding failures of geosynthetic landfill cover slopes are common and often due to improper drainage of infiltrating water. Landfill cover failures may be small and are frequently repaired without being reported or studied. However, modern landfills can be massive, and they have the potential for large cover slope failures that are expensive to repair and potentially dangerous.

1.2 EXAMPLE CASE

The example landfill cover is representative of modern landfill cover design and construction in the US. The final cover suffered a sliding failure during construction, resulting in litigation that has not yet been resolved. Because of the pending litigation, details such as the landfill location and owner will not be provided.

1.2.1 Example Cover System

The example cover system is representative of current practice and consists of a protective soil layer and a geosynthetic drainage layer overlying a composite hydraulic barrier made of a textured geomembrane and compacted clay (Figure 1.1). Note that the

drainage outlet consists only of the geocomposite drainage layer daylightling out of the cover slope.

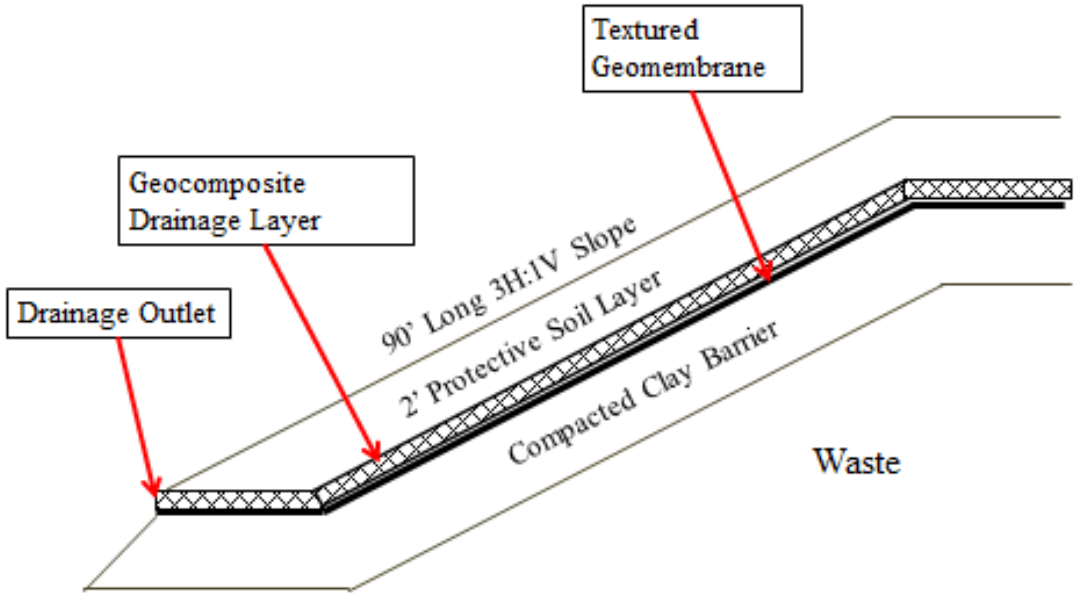

Figure 1.1: Cross-section showing example cover system components (not to scale)

1.2.2 Example Case Sliding Failure

The example landfill cover suffered a sliding failure with the slip surface along the geosynthetic drainage layer/textured geomembrane interface (Figure 1.2). The sliding failure was discovered the day after 0.7 inches of rainfall were recorded at the weather station nearest the landfill. It was observed during the site investigation that:

- The geosynthetic drainage layer did not daylight in intact sections of the slope. In general the drainage material was covered by soil and sandbags at the toe of the slope and only visible in isolated locations.

- The condition of the drainage outlet in failed sections of the slope could not be determined because it was covered by the slide.
- The geosynthetic drainage layer was partly exposed at the time of the slide. Specifically, drainage material at the crest of the slope was left uncovered in both intact and failed sections of the cover.

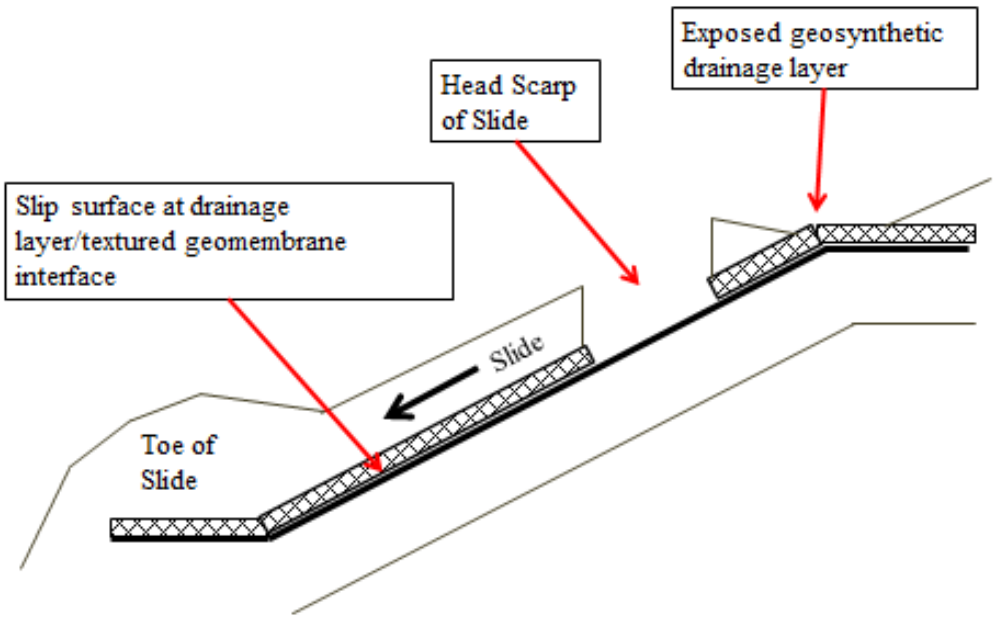

Figure 1.2: Cross-section of example case sliding failure

The absence of protective soil at the crest of the slope allowed rainfall to enter the drainage layer directly, without having to infiltrate through the protective soil layer. Also, the soil and sandbags covering the drainage layer outlet constrained the flow of water exiting the drainage layer. After the failure, experimental testing determined that geocomposite drainage material and textured geomembrane from the failed section of the slope retained over 90% of the peak interface shear strength measured for virgin

materials, despite displacing many feet during the slide. Prior to installation, testing had determined that fully mobilized large displacement interface shear strength was only 70% of the peak interface shear strength at normal stresses similar to the overburden from the protective soil layer.

1.3 RESEARCH OBJECTIVES

The objectives of this project are to:

- Summarize regulation and the current state of practice in landfill cover design, focusing on the design of drainage layers and drainage layer outlets.
- Using experimental methods, investigate geosynthetic landfill cover materials' behavior as cover systems approach failure.
- Develop analytical and numerical methods for analyzing the hydraulic behavior of geosynthetic drainage layers with constrained flow at the outlet.
- Develop a landfill cover slope stability model that satisfies force equilibrium and strain compatibility while taking into account various pore water pressure conditions and effective normal stress dependent strain softening of interfaces.

1.4 ORGANIZATION OF THESIS

This document is divided into six chapters. After the introduction, background information is presented in Chapter 2. Relevant background information includes regulatory guidelines that dictate MSW landfill cover design and example designs of cover drainage layers and drainage layer outlets. In Chapter 3 presents two experimental studies that were conducted for this research project. Tensile tests were conducted to determine the axial tensile stiffness of a geocomposite drainage layer, and inclined plane tests were conducted to characterize the shear strength and normal stress dependent strain-softening of a geocomposite/textured geomembrane interface.

Chapter 4 focuses on hydraulic modeling. A simple hydrostatic example is used to demonstrate the difference in water storage capacity of geosynthetic drainage layers compared to granular drainage layers. Then, a numerical method is presented to model confined flow in the drainage layer with constrained flow at the outlet.

In Chapter 5, a slope stability model is presented that uses iterative numerical methods to calculate stability solutions that satisfy force equilibrium and strain compatibility. The strain compatible slope stability model uses a variety of assumed and calculated pore water pressure conditions in the drainage layer and takes into account the normal stress dependent strain softening of the drainage material/textured geomembrane interface.

Finally, conclusions and recommendations for future research are presented in Chapter 6.

CHAPTER 2: BACKGROUND

2.1 INTRODUCTION

The design, construction, operation, and closure of new solid waste containment facilities in the United States are governed by the Resource Conservation and Recovery Act (RCRA), which was first passed in 1976. The origins of current regulation may be traced to draft regulations for hazardous waste containment released in 1982 and promulgated in 1984. In 1993, regulations for hazardous waste containment were largely adopted for municipal solid waste containment.

At the federal level, regulations are contained in the Code of Federal Regulations (CFR), and the regulator tasked with enforcement is the United States Environmental Protection Agency (EPA). Regulations governing municipal solid waste are covered by RCRA Subtitle D and contained in 40 CFR Part 258, and regulations governing hazardous waste are covered by RCRA Subtitle C and contained in 40 CFR Part 260. This research report focuses on final covers for municipal solid waste landfill facilities (MSWLF), but the experiments, analysis, and conclusions are also relevant for hazardous waste containment facilities.

The EPA may authorize states to adopt their own regulations, but state guidelines must be at least as restrictive as federal guidelines. In Texas, regulations are contained in the Texas Administrative Code and enforced by the Texas Commission on Environmental Quality.

2.2 LANDFILL COVER DESIGN REGULATION

RCRA guidelines tend to be prescriptive, meaning they largely dictate design. At the federal level, regulations for municipal solid waste final cover design are contained in 40 CFR 258.60(a):

> Statement of Regulation
>
> (a) Owners or operators of all MSWLF units must install a final cover system that is designed to minimize infiltration and erosion. The final cover system must be designed and constructed to:
>
> (1) Have permeability less than or equal to the permeability of any bottom liner system or natural subsoils present, or a permeability no greater than 1 x 10^{-5} cm/s, whichever is less, and
>
> (2) Minimize infiltration through the closed MSWLF unit by the use of an infiltration layer that contains a minimum of 18-inches of an earthen material, and
>
> (3) Minimize erosion of the final cover by the use of an erosion layer that contains a minimum 6-inches of earthen material that is capable of sustaining native plant growth.

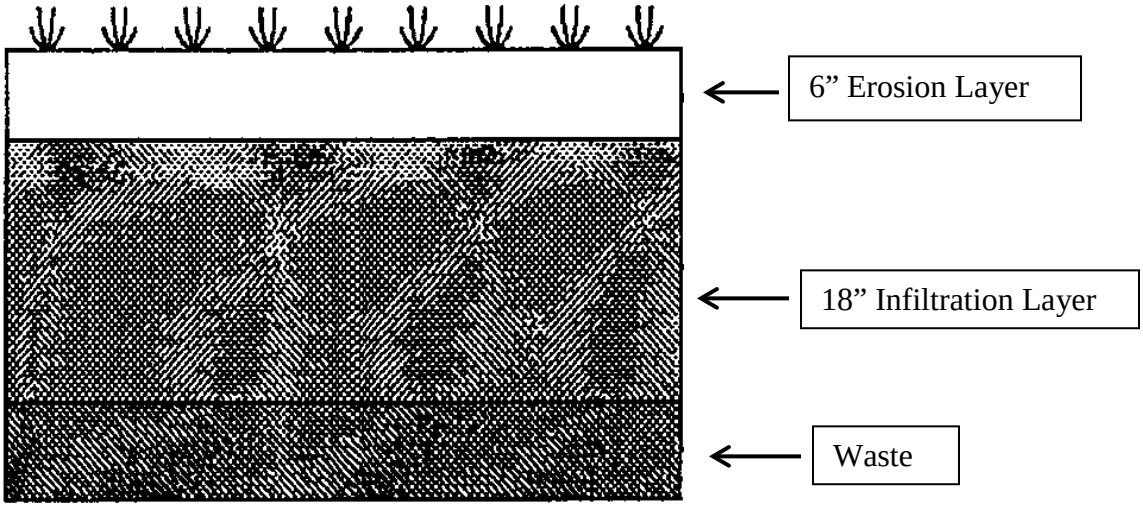

Figure 2.1: Minimum RCRA Subtitle D final cover system

RCRA Subtitle D does not require a drainage layer be included in the final cover system, but many state regulators either require or recommend a drainage layer above the infiltration layer. For example, based upon, "various federal guidelines and the Ohio EPA's experience with closures, the Ohio EPA's recommended design of a RCRA final cover…calls for":

(a) First low permeability layer-- a two foot-thick layer of recompacted clay with a maximum permeability of $1x10^{-7}$ cm/s;

(b) Second low permeability layer-- a flexible membrane liner (40 mil minimum thickness, or more if required for successful welding, if HDPE is used, or 40 mil if another suitable material is used.);

(c) Drainage layer-- at least 12 inch-thick soil drainage layer with a minimum permeability of $1x10^{-2}$ cm/s, or an equivalent geosynthetic drainage layer; and

(d) Protection layer-- at least 18 inch-thick soil vegetative/frost protection layer.

(Ohio EPA, 2000)

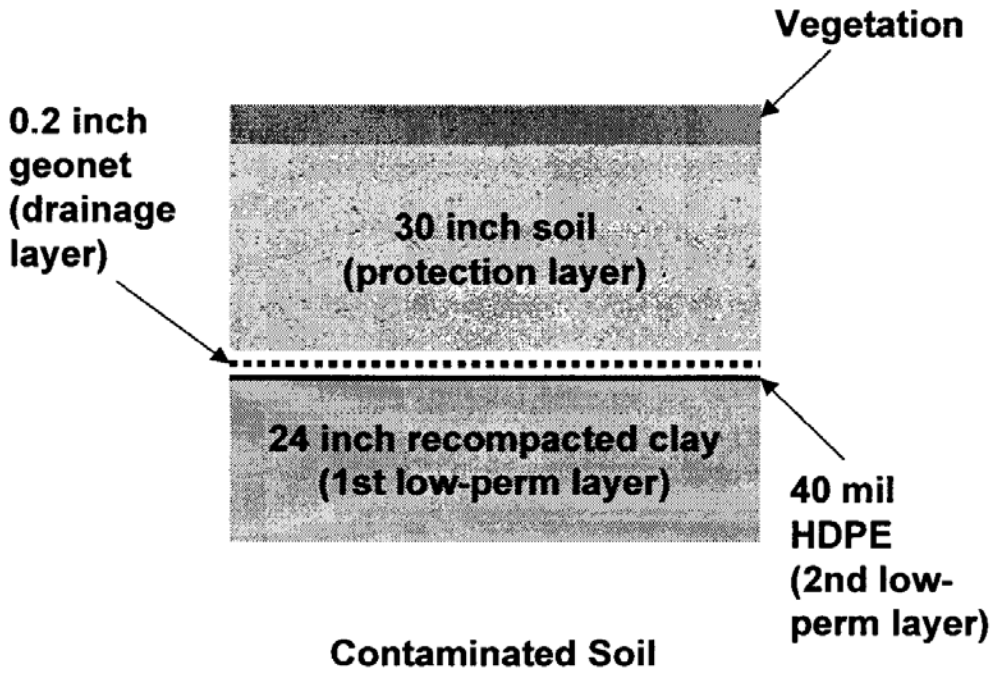

Figure 2.2: Ohio EPA's recommended RCRA Subtitle D final cover system (Ohio EPA, 2000)

The permeable drainage layer is intended to remove water from above the low-permeability infiltration layer and reduce the potential for leachate generation. While RCRA Subtitle D does not mandate a drainage layer, it does provide design regulation should a drainage layer be included in a final cover system:

> If granular drainage layer material is used, the filter layer should be at least 12-in thick with a hydraulic conductivity in the range of $1x10^{-2}$ cm/s to $1x10^{-3}$cm/s…
>
> If geosynthetic materials are used as a drainage layer, the fully saturated effective transmissivity should be the equivalent of 12 inches of soil with a hydraulic conductivity range of $1x10^{-2}$ cm/s to $1x10^{-3}$cm/s
>
> (40 CFR 258.60(b))

A seminar publication from the EPA states that if a geosynthetic drainage layer is used, “all of the infiltrating surface water that is collected from the geonet or geocomposite sheet drain is conveyed to the perimeter of the closure, where it is collected in a perforated pipe or in a geocomposite edge drain” (U.S. EPA, 1991). Similarly, the Ohio EPA recommends (but does not require), that “the drainage layer must have a free exit flow to a designed ditch, sewer, or other structure capable of handling maximum expected flow” (Ohio EPA, 2000). However, RCRA Subtitle D regulation does not require that the drainage layer have a designed outlet, nor does it provide design guidelines for the drainage layer outlet.

2.3 EXAMPLE COVER DESIGNS

Examples are presented to show the current state of practice in the design of final cover systems and drainage layer outlets for new MSW landfill facilities. All of the designs were approved by TCEQ and are public record.

2.3.1 Final Cover Cross Sections

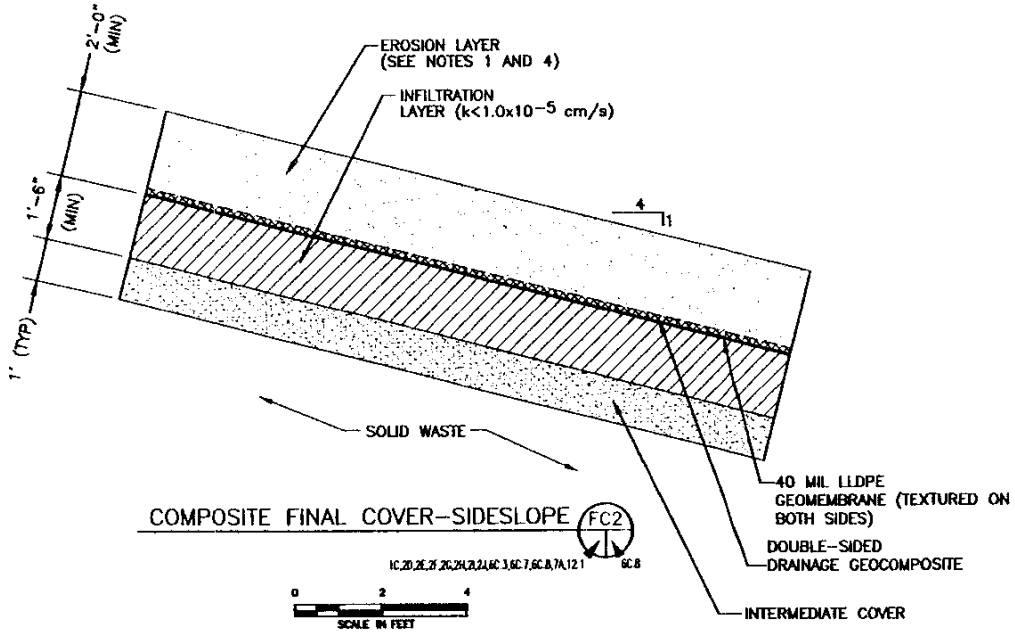

Figure 2.3: Blue Ridge Landfill final cover (Weaver Boos, 2005)

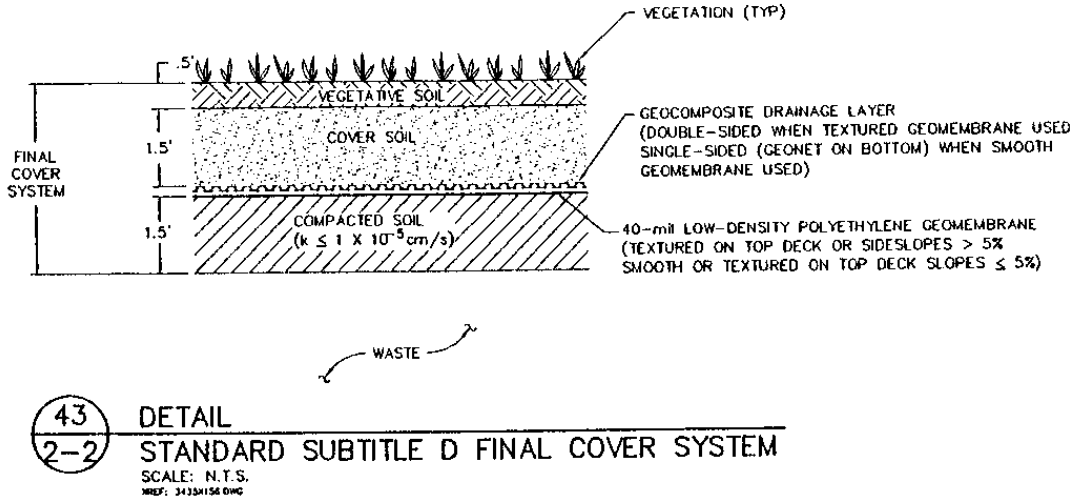

Figure 2.4: Mesquite Creek Landfill final cover (Geosyntec, 2006)

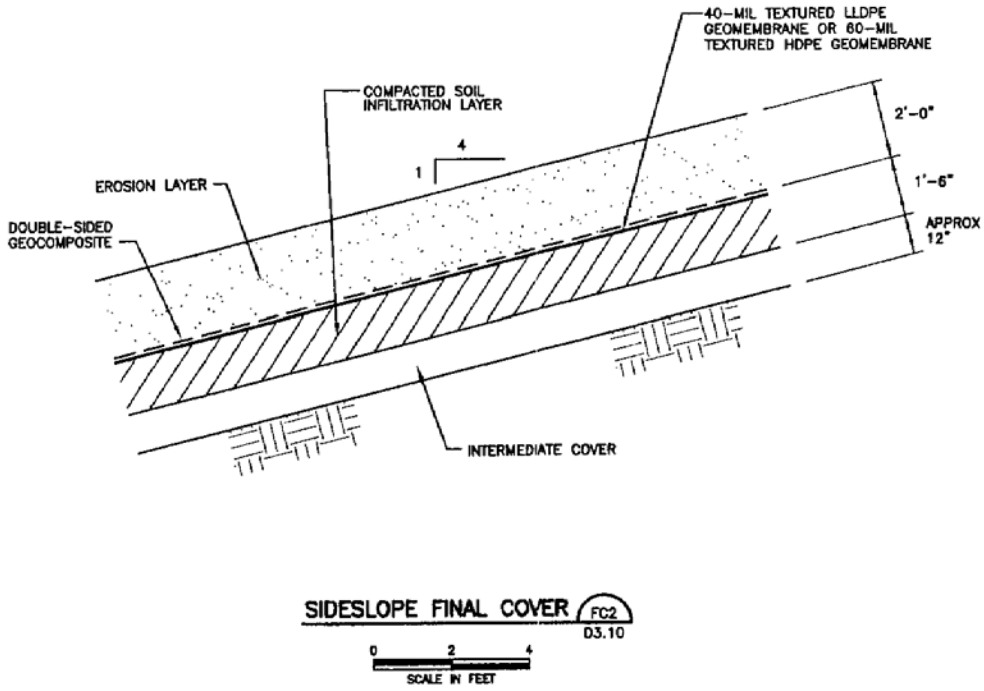

Figure 2.5: IESI East Texas Regional Landfill final cover (Biggs & Mathews, 2009)

2.3.2 Cover Drainage Outlet Details

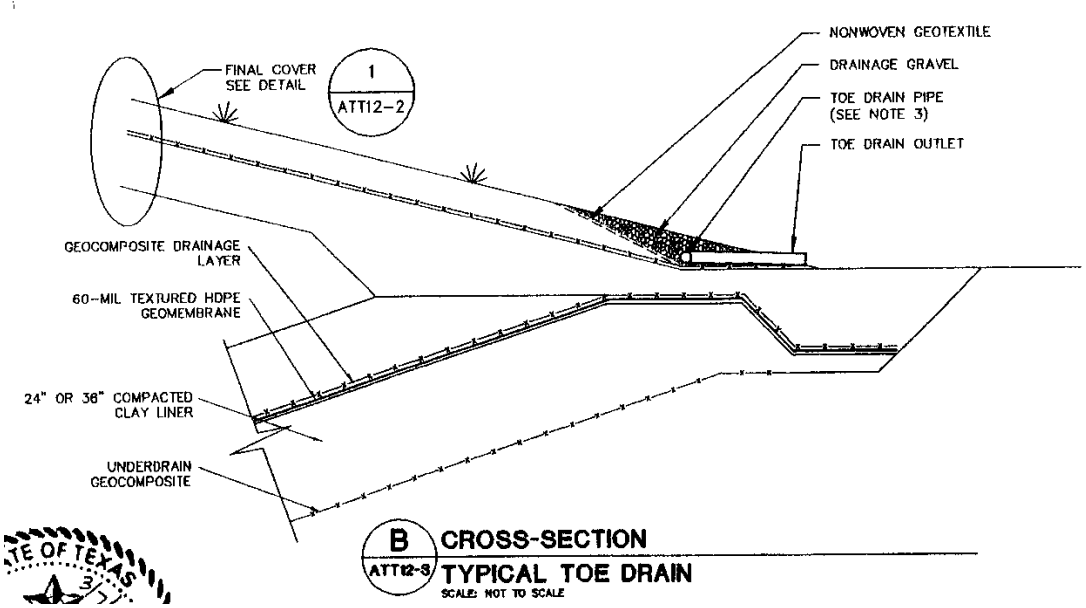

Figure 2.6: Seabreeze Environmental Landfill drainage outlet detail (Golder, 2001)

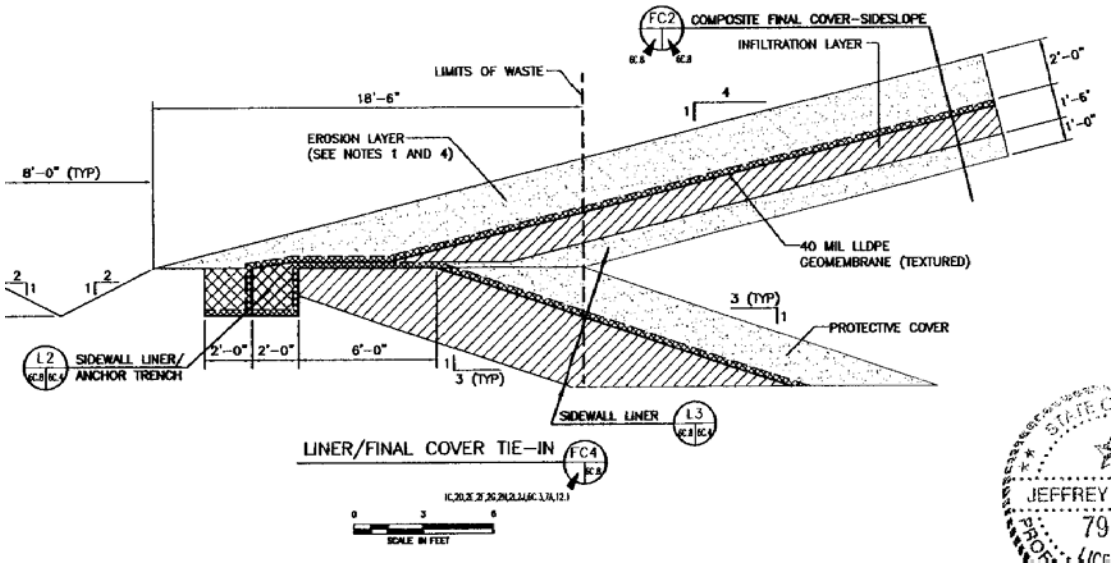

Figure 2.7: Blue Ridge Landfill drainage outlet detail (Weaver Boos, 2005)

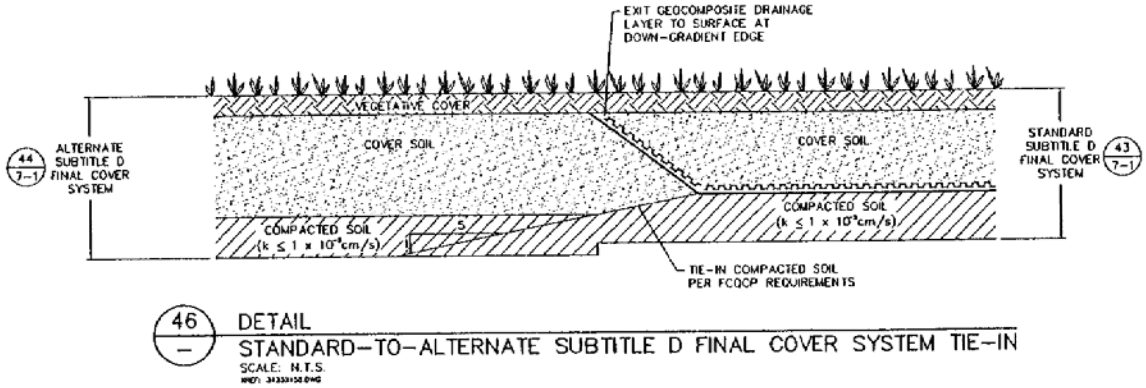

Figure 2.8: Mesquite Creek Landfill drainage outlet detail (Geosyntec, 2006)

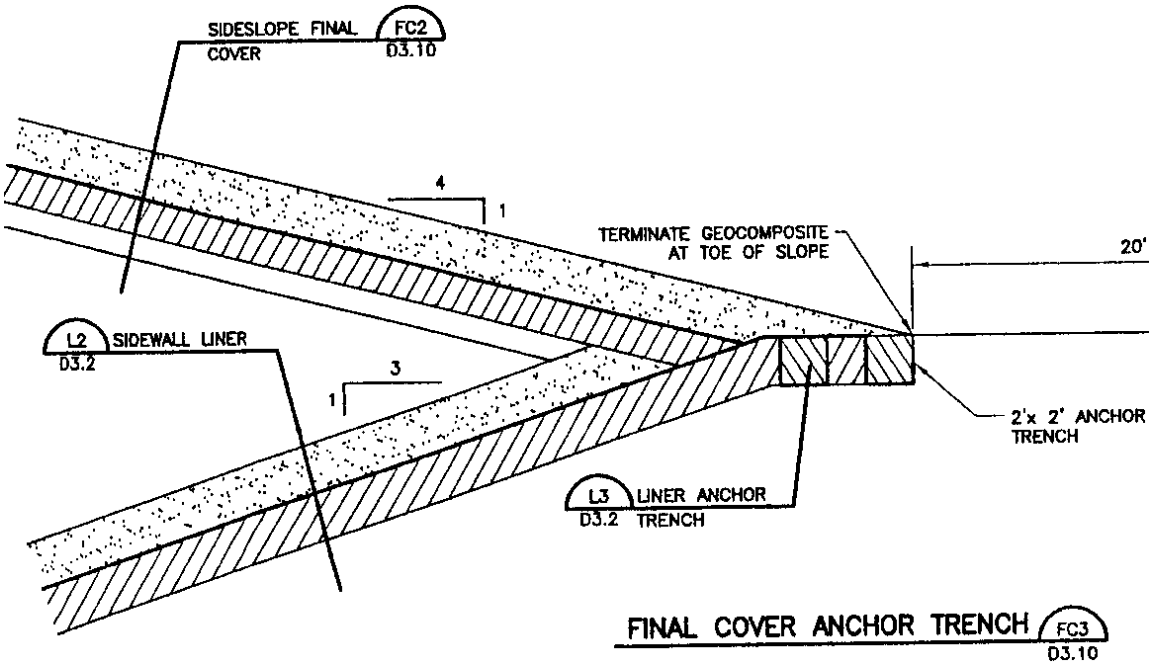

Figure 2.9: IESI East Texas Regional Landfill drainage outlet detail (Biggs & Mathews, 2009)

2.4 DISCUSSION

RCRA Subtitle D requires that new landfill bottom liners contain a composite hydraulic barrier layer consisting of a geomembrane in intimate contact with 2-ft of compacted clay having hydraulic conductivity no greater than $4.0*10^{-8}$ in/s (10^{-7} cm/s) (40 CFR 258.40). By requiring that the landfill cover be equally or less permeable than the bottom liner, RCRA essentially mandates a composite infiltration barrier layer for the cover system of new facilities. Also, by including design guidelines for cover drainage layers, and by equating granular and geosynthetic drainage layers by their saturated hydraulic conductivities, the current state of practice is to include a geosynthetic drainage layer in the cover system even though it is not explicitly mandated by RCRA. The final cover cross section designs presented in section 2.3.1 are nearly identical to one another

and consist of protective cover soil and a geosynthetic drainage layer overlying a composite infiltration barrier layer, just like the example case presented in Chapter 1.

However, while cover system cross-sections have very little variety from one design to the next, there are huge differences between designs of drainage layer outlets. The drainage layer outlet may be highly designed and include granular material and perforated pipe, as in Figure 2.6, or the outlet may be almost not designed at all, consisting only of the drainage material daylighting, as in Figure 2.8, Figure 2.9, and the example slope from Chapter 1. The importance of designing the drainage layer outlet to ensure free flow of water out of the drainage layer is addressed in the technical guidance document for hazardous waste landfill cover design (US EPA, 1989): "the drainage layer must slope to an exit drain which allows percolated water to be efficiently removed." The US EPA also provides recommendations for geopipe and geocomposite "edge drain" design to be used with geocomposite drainage layers in a seminar publication (1991). However, neither the importance of drainage outlet design, nor outlet design guidelines are included in the RCRA Subtitle D *regulation*.

Modern landfill designs generally include geosynthetic drainage layers, but they often lack designed systems at the drainage layer outlet. The absence of a designed system to ensure free flow at the outlet makes clogging or other constraints to flow out of the drainage layer more likely. This suggests RCRA should explicitly require a designed outlet if a drainage layer is included, or at least give design guidelines for the drainage outlet in the regulation, not just in guidance documents.

CHAPTER 3: EXPERIMENTAL INVESTIGATION OF GEOSYNTHETIC MATERIAL BEHAVIOR AS COVER SYSTEM APPROACHES FAILURE

3.1 INTRODUCTION

Two experimental studies were conducted for this research project: wide width tensile tests and inclined plane tests. The experiments were conducted to investigate the behavior of landfill cover systems approaching a sliding failure along the geocomposite drainage material/textured geomembrane interface. In this type of sliding failure, deflections in the cover system result in tension in the geocomposite material and displacement in the drainage material relative to the textured geomembrane. Wide width tensile tests were conducted to determine the tensile strength and stiffness of a geocomposite drainage material, and tilt table tests were conducted to characterize the shear strength of a geocomposite drainage material/textured geomembrane interface.

3.2 GEOSYNTHETIC MATERIALS

Geosynthetic materials representative of the current state of practice in landfill cover design and construction were selected for this research project. SKAPS TN 270-2-6 geocomposite drainage material and Poly-Flex 40-mil textured LLDPE geomembrane were obtained.

3.2.1 SKAPS TN 270-2-6 Geocomposite Drainage Material

SKAPS Transnet 270-2-6 geocomposite is a sheet drain material that consists of, "SKAPS GeoNet made from HDPE resin with non-woven polypropylene geotextile fabric heat bonded on both sides of GeoNet" (www.skaps.com). The geonet is 270-mil thick, and the non-woven geotextile has a weight of 6 ounces per square yard. Properties

of TN 270-2-6 reported by SKAPS are shown in Figure 3.1, and a picture of a roll of TN 270-2-6 is shown in Figure 3.2.

Property	Test Method	Unit	Required Value		Qualifier
			With 6 oz.	With 8 oz.	
Geonet					
Thickness	ASTM D 5199	mil.	270±15	270±15	Range
Carbon Black	ASTM D 4218	%	2 to 3	2 to 3	Range
Tensile Strength	ASTM D 5035	lb/in	75	75	Minimum
Melt Flow	ASTM D 1238[3]	g/10 min.	1	1	Minimum
Density	ASTM D 1505	g/cm^3	0.94	0.94	Minimum
Transmissivity[1]	ASTM D 4716	$m^2/sec.$	$3x10^{-3}$	$3x10^{-3}$	MARV[2]
Composite					
Ply Adhesion (Minimum)	ASTM D7005	lb/in	0.5	0.5	MARV
Ply Adhesion (Average)	ASTM D7005	lb/in	1	1	MARV
Transmissivity[1]	ASTM D 4716	m^2/sec	$5x10^{-4}$	$5x10^{-4}$	MARV
Geotextile					
Fabric Weight	ASTM D 5261	oz/yd^2	6	8	MARV
Grab Strength	ASTM D 4632	lbs	160	225	MARV
Grab Elongation	ASTM D 4632	%	50	50	MARV
Tear Strength	ASTM D 4533	lbs	65	90	MARV
Puncture Resistance	ASTM D 4833	lbs	95	130	MARV
CBR Puncture	ASTM D 6241	lbs	475	650	MARV
Water Flow Rate	ASTM D 4491	gpm/ft^2	125	100	MARV
Permittivity	ASTM D 4491	sec^{-1}	1.63	1.26	MARV
Permeability	ASTM D 4491	cm/sec	0.3	0.3	MARV
AOS	ASTM D 4751	US Sieve	70	80	MARV

Figure 3.1: Transnet 270-2-6 properties reported by SKAPS Industries (www.skaps.com)

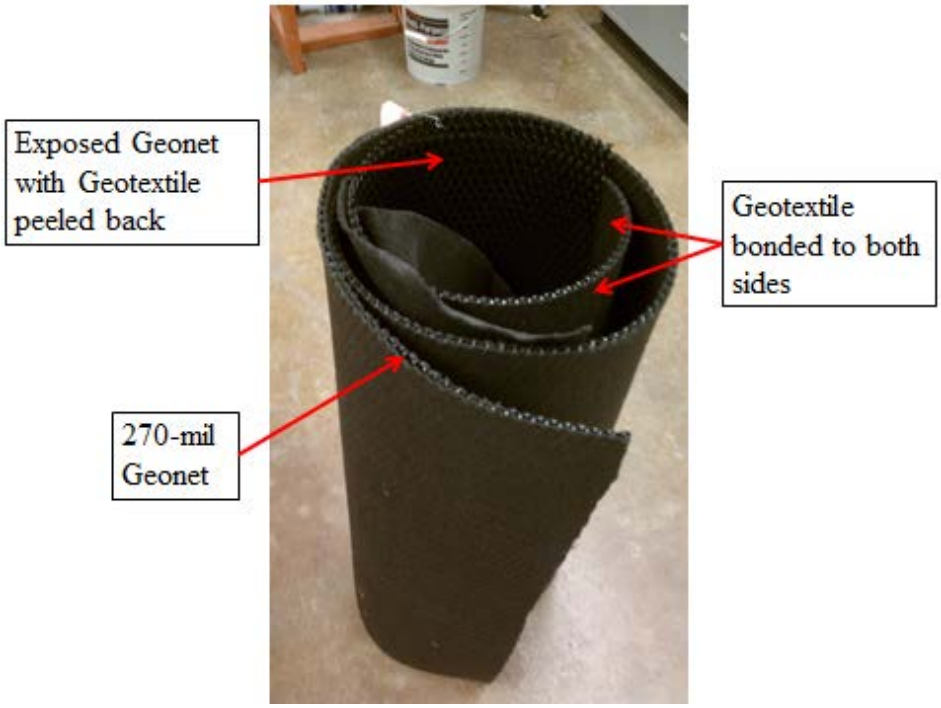

Figure 3.2: Picture of SKAPS TN 270-2-6 geocomposite drainage material

3.2.2 Poly-Flex 40-mil LLDPE Textured Geomembrane

The Poly-Flex 40-mil LLDPE textured geomembrane was textured on both sides and made of linear low density polyethylene (LLDPE). Low density polyethylene geomembranes are often used in landfill cover systems because they are more flexible than high density polyethylene (HDPE) geomembranes and better able to withstand deformation from gas pressures and differential settlement.

		Minimum Average Values		
Property	Test Method	40 Mil	60 Mil	80 Mil
Thickness, mils	ASTM D 5994			
minimum average		38	57	76
lowest individual of 8 of 10 readings		36	54	72
lowest individual of 10 readings		34	51	68
Asperity Height[1], mils	ASTM D 7466	10	10	10
Sheet Density, g/cc (max.)	ASTM D 1505/D 792	0.939	0.939	0.939

Figure 3.3: 40-mil textured LLDPE geomembrane properties reported by Poly-Flex (www.poly-flex.com)

3.3 TENSILE TESTS

As shown in Figure 3.1, the tensile strength of the geonet was provided by SKAPS, but the tensile strength and stiffness of the composite material were not provided. Four tensile tests were conducted to determine the tensile strength and stiffness of the SKAPS TN 270-2-6 geocomposite drainage material.

3.3.1 Equipment

A Satec Systems 60,000 lb capacity load frame was used to conduct the tensile tests. Roller grips were used to secure the geocomposite drainage layer, an Omega load cell model LCCA-5K with a 5,000 lb capacity was used to measure tensile force, and an Omega model LD620-50 LVDT was used to measure the length of the geocomposite sample. Labview 2009 was used to collect data from the load cell and LVDT.

3.3.2 Methods

The methods used to conduct the tensile tests were similar to ASTM D4595-09, the standard wide width tensile test for geotextiles. Using a utility knife, four sample strips were cut with widths 8 in, 5 in, 5.5 in, and 8 in. The target parameter was axial stiffness in the machine direction, so sample width was measured in the cross-machine direction for all samples. The strips were inserted centrally in roller grips, and the strain gauge was attached with an initial length of 4 inches. The load frame was set to displace 0.4 in/min (1 cm/min), and all samples were elongated until the maximum displacement of the load frame was reached.

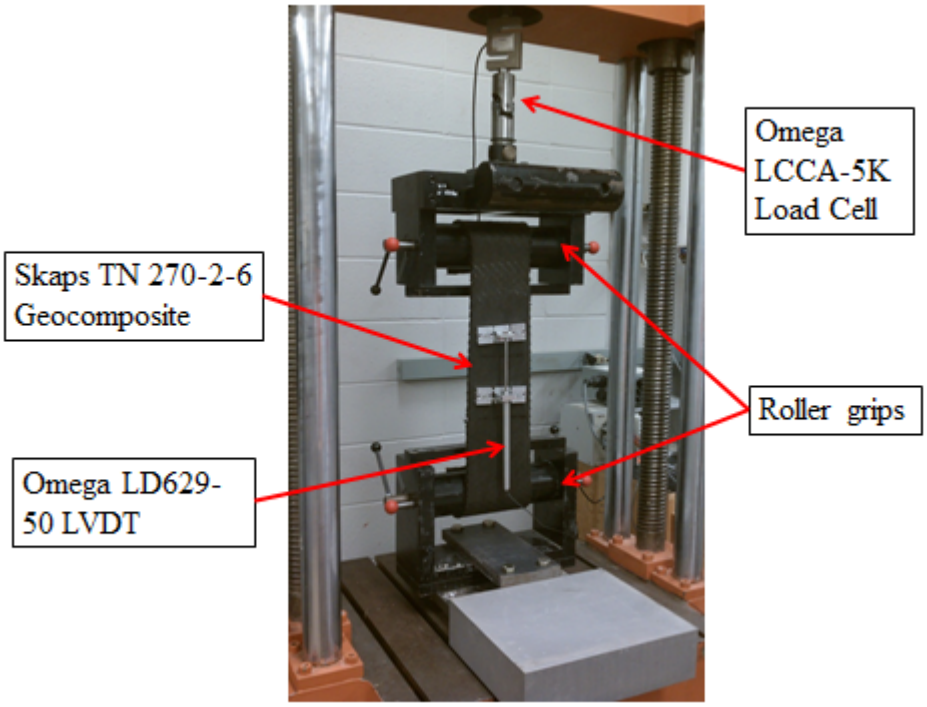

Figure 3.4: Picture of tensile test of SKAPS TN 270-2-6 geocomposite

3.3.3 Results

Wide width tensile test results of are shown in Figures 3.5 through 3.9. None of the samples reached its tensile strength within the travel of the testing equipment. The axial stiffness was approximately linear and was estimated to be 180 lbs per inch width, or 2,200 lbs per foot width.

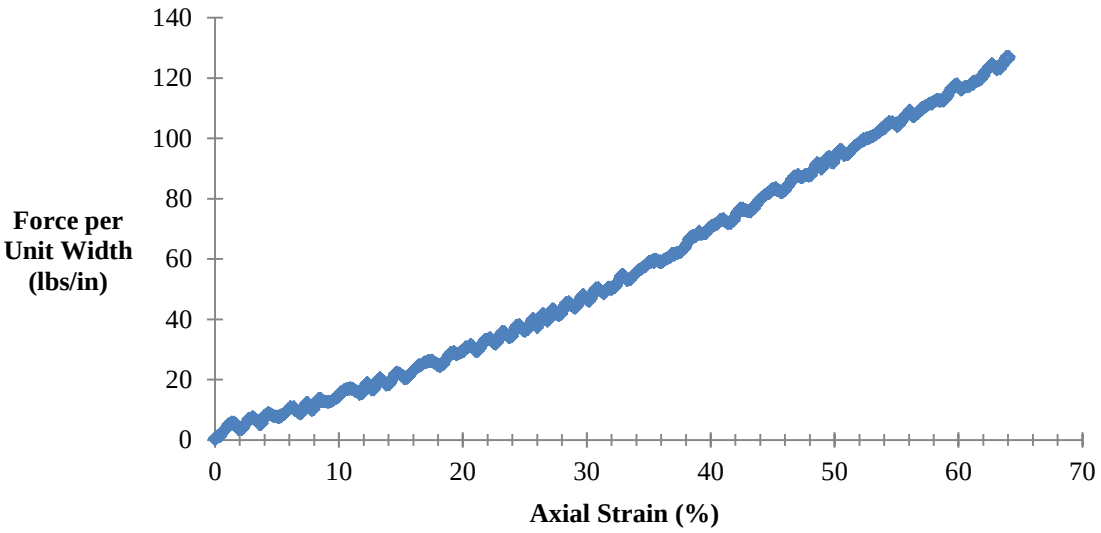

Figure 3.5: Tensile test results for 8-in wide sample of SKAPS TN 270-2-6

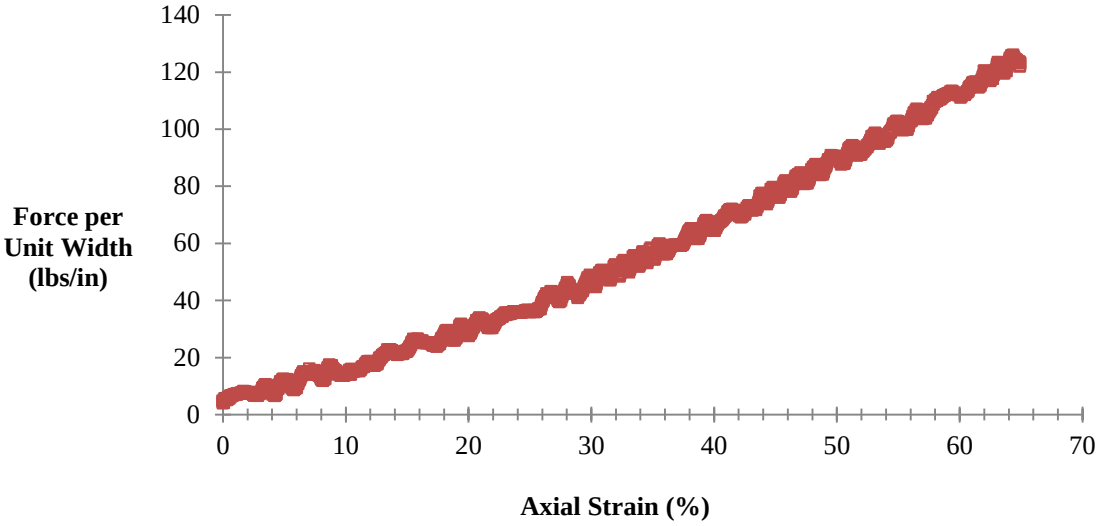

Figure 3.6: Tensile test results for 5-in wide sample of SKAPS TN 270-2-6

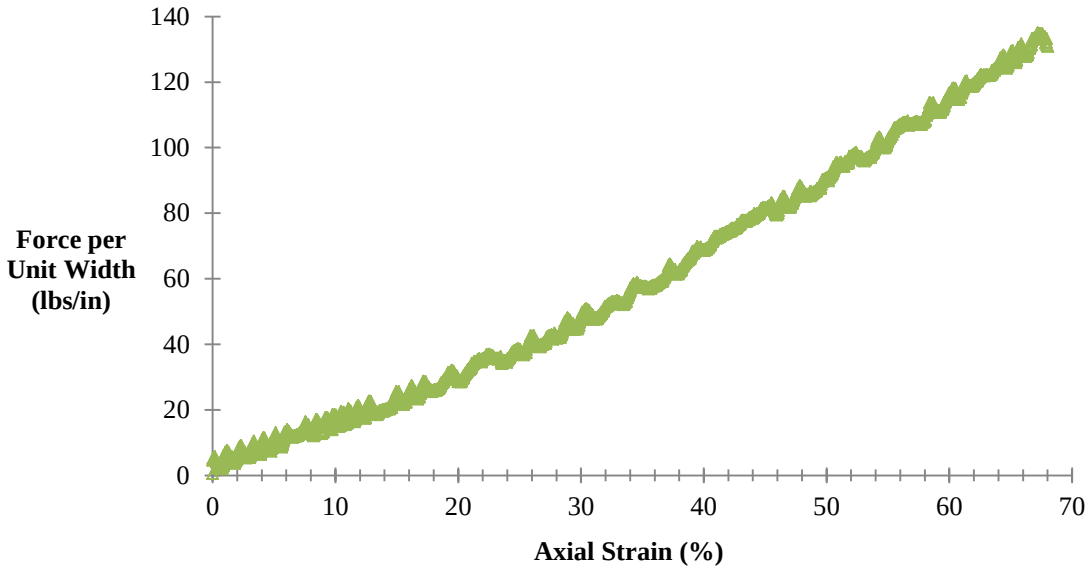

Figure 3.7: Tensile test results for 5.5-in wide sample of SKAPS TN 270-2-6

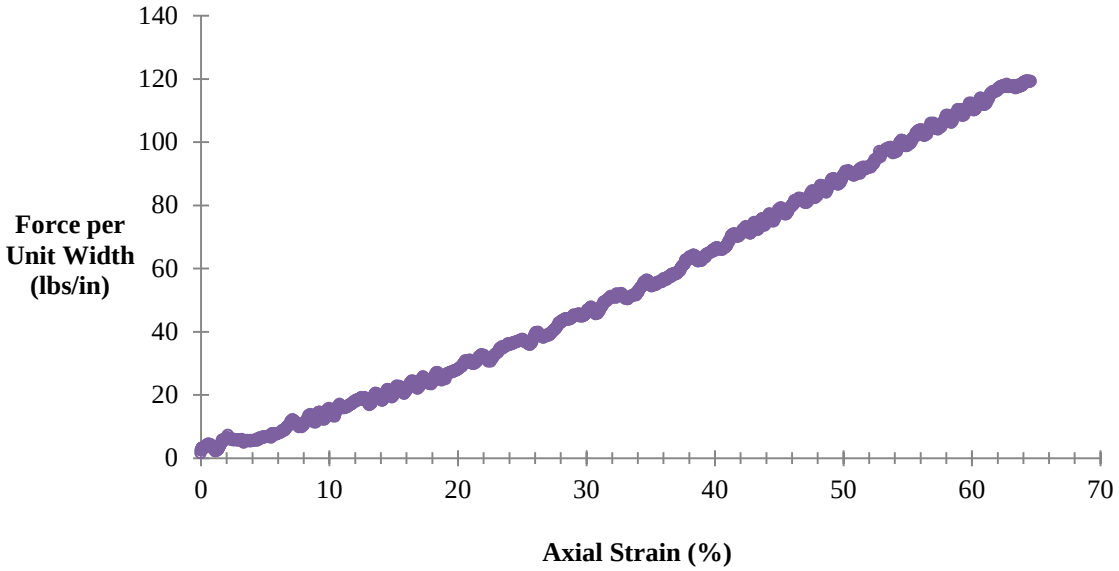

Figure 3.8: Tensile test results for 8-in wide sample of SKAPS TN 270-2-6

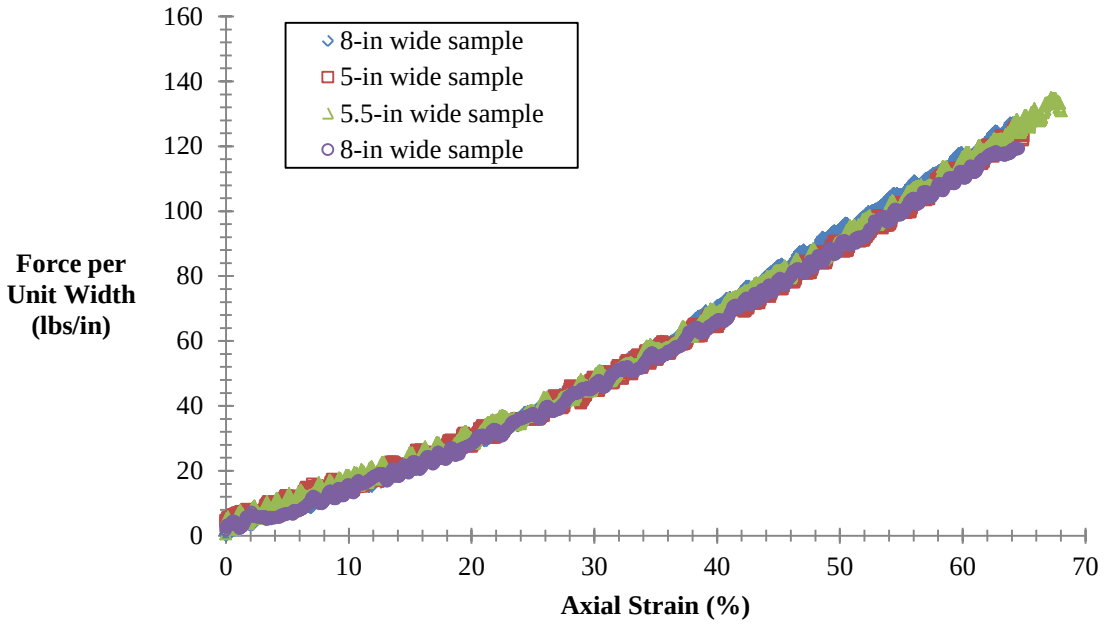

Figure 3.9: Tensile test results for all samples of SKAPS TN 270-2-6

3.3.4 Discussion

While the axial stiffness was determined using the wide width tensile tests, the ultimate tensile strength could not be determined within the travel of the load frame. Essentially, each trial turned out to be a proof load test. The lowest maximum unit tension of the four tests was 120 lbs/in, which is 60% greater than the tensile strength reported by SKAPS for the 270 mil HDPE geonet. The greater strength determined for the geocomposite material compared to the reported value for the geonet alone may be due to the heat-bonded non-woven geotextiles. The greater tensile strength measured may also be because the value published by SKAPS is a "Minimum Average Roll Value" (MARV), which is the defined as the value such that a user/purchaser of the product will have 97.7% confidence that the product will meet or exceed the published value.

3.4 INCLINED PLANE TESTS

Inclined plane tests were conducted to characterize the interface shear strength between SKAPS TN 270-2-6 geocomposite drainage material and Poly-Flex 40-mil LLDPE textured geomembrane.

3.4.1 Geosynthetic Interface Shear Strength Background

It has been determined that textured geomembrane/non-woven geotextile interfaces exhibit strain softening behavior, meaning the shear strength mobilized at the interface decreases with displacement after a maximum, or peak, shear stress is reached (Gilbert et al, 1995; Li, 1995). It has also been observed that the decrease in shear stress from the maximum value to the large-displacement value depends on the effective normal stress at which the materials were sheared (Gilbert and Byrne, 1996). For instance, large scale direct shear tests on an HDPE textured geomembrane/HDPE non-woven geotextile interface showed that samples sheared under 16 kPa effective normal stress did not exhibit strain softening, but samples sheared under 340 kPa and 690 kPa did exhibit strain softening (Figure 3.10). Further, the available interface shear strength of samples displaced under 16 kPa effective normal stress did not decrease when they were re-tested multiple times. In contrast, samples sheared under 340 kPa and 690 kPa effective normal stress had reduced peak interface shear strength when re-tested, and the available interface shear strength of previously sheared materials was approximately equal to the large-displacement shear stress of the previous test.

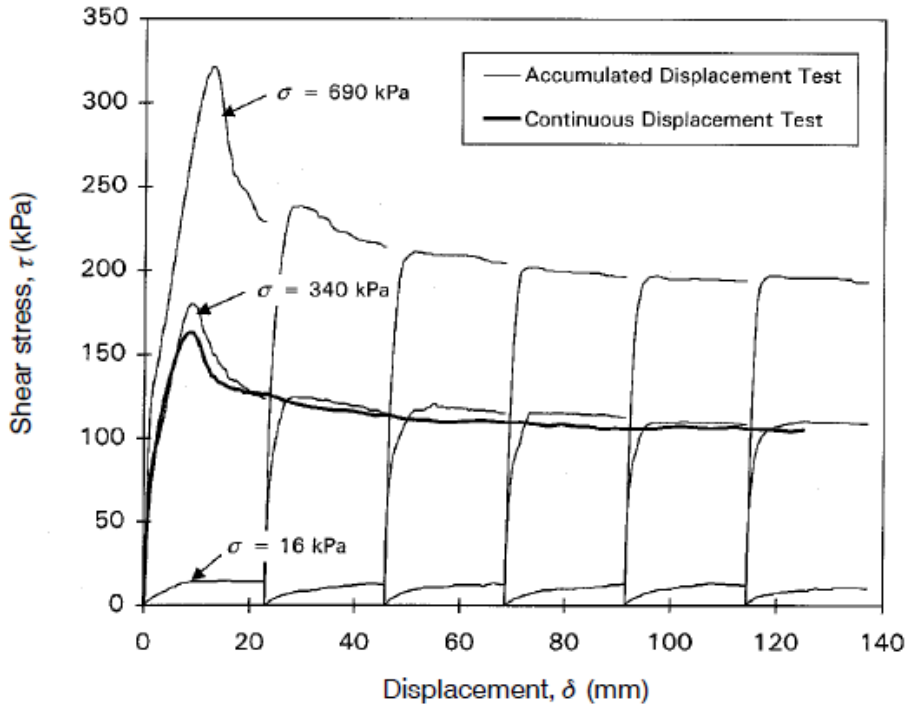

Figure 3.10: Accumulated displacement results from direct shear tests of a non-woven geotextile/textured geomembrane interface (Li, 1995)

The previous research cited focused on geosynthetic interface behavior when materials are displaced at a constant normal stress or re-tested at the same normal stress. The purpose of the inclined plane testing in this research project is to characterize the available shear strength of a geosynthetic interface when materials are re-tested at normal stresses *different* than the normal stress at the virgin materials were sheared.

3.4.2 Equipment

A hand-operated tilt table device was used to conduct the inclined plane tests. The tilt table consisted of a flat, rectangular 24-inch x 18-inch metal tray hinged to a steel frame along one of the shorter sides. A strap connected the metal tray with a geared hand crank used to raise the side of the tray opposite the hinge. The hand crank included a ratchet mechanism that held the tray at a constant inclination. A wooden loading platen

was constructed to apply a uniform normal stress at the interface when the tray was inclined 29° (Figure 3.11).

3.4.3 Methods

Using a utility knife, samples of SKAPS TN 270-2-6 geocomposite measuring 4 inches in the cross machine direction by 8-inches in the machine direction were cut from the roll. Also using a utility knife, samples of Poly-Flex 40-mil LLDPE textured geomembrane measuring 18-inches by 18-inches were cut from the roll. The tilt table was leveled in its fully lowered position, and the geomembrane was secured to the tilt table in the machine direction using clamps at all four corners. A geocomposite sample was placed on the geomembrane in the machine direction, the loading platen was placed on the geocomposite sample, and weights were added to the loading platen. After weights were added to the loading platen, the sample was given 2 minutes to seat. After seating, the inclination of the tilt table was increased at a rate of approximately 1°/min until the geocomposite sample slid down the geomembrane. The angle of the tilt table was recorded as the peak secant friction angle for that trial. The procedure was repeated with the same samples, with care taken that the geocomposite was placed in the same initial position on the geomembrane. Each pair of samples was tested twice. In the first trial, the materials had not been sheared and were considered “virgin”. In the second trial, the materials were no longer “virgin”, because they had been sheared in the first trial.

Table 3.1: Inclined plane test matrix

		Weight on Loading Platen, 2nd Trial			
		10 lbs	20 lbs	30 lbs	40 lbs
Weight on Loading Platen, 1st Trial	10 lbs	X	X	X	X
	20 lbs	X	X	X	X
	30 lbs	X	X	X	X
	40 lbs	X	X	X	X

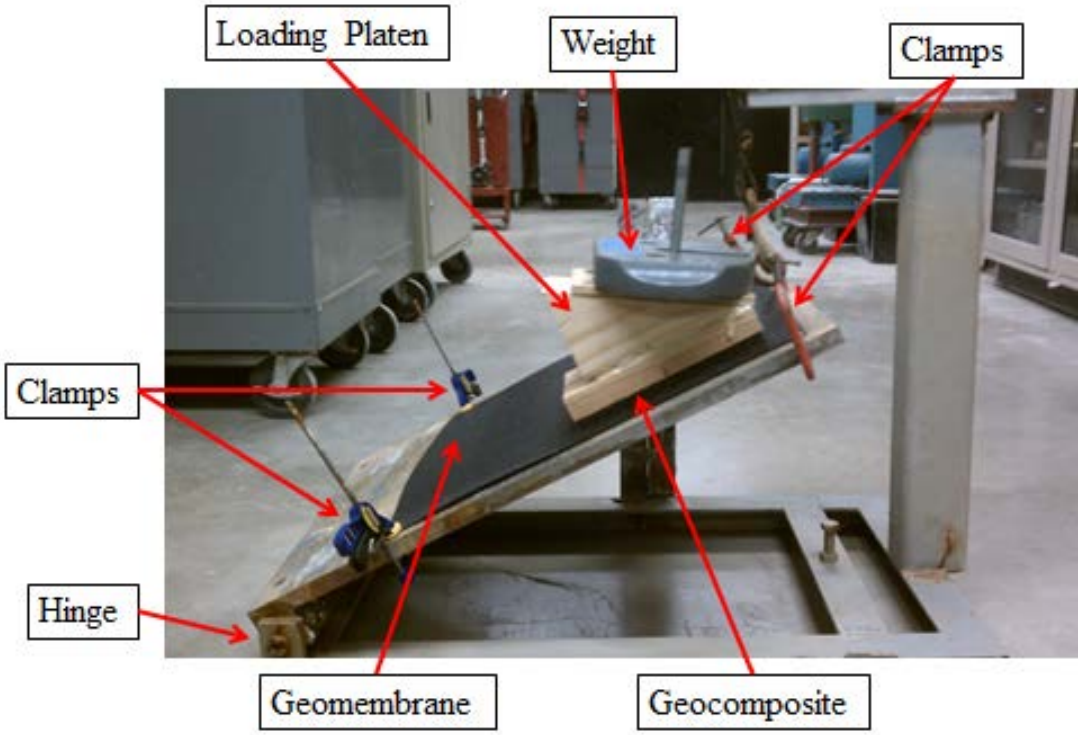

Figure 3.11: Picture of inclined plane test before sliding

Figure 3.12: Picture of inclined plane test after sliding has occured

3.4.4 Results

Over the range of effective normal stresses investigated, interface shear strength envelopes for virgin materials and re-tested materials were linear and had little or no apparent cohesion. The available shear strength at an interface previously sheared under 50-60 psf effective normal stress was nearly unchanged from the virgin materials' interface shear strength (Figures 3.14, 3.15, 3.19). Materials previously sheared under 90 psf effective normal stress or greater had reduced interface shear strength available when re-tested under various effective normal stresses (Figures 3.13, 3.16, 3.17, 3.18, 3.19). Materials previously sheared under 150-155 psf effective normal stress and 195 – 200 psf effective normal stress had nearly identical available interface shear strength envelopes when the materials were re-tested at various normal stresses (Figures 3.17, 3.18, 3.19).

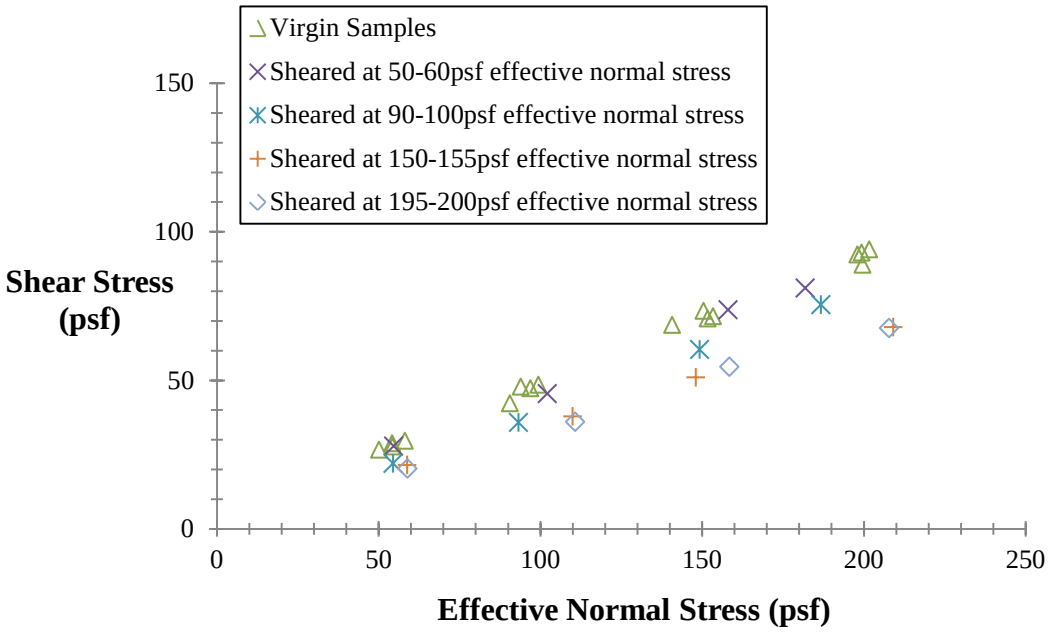

Figure 3.13: Results of inclined plane tests

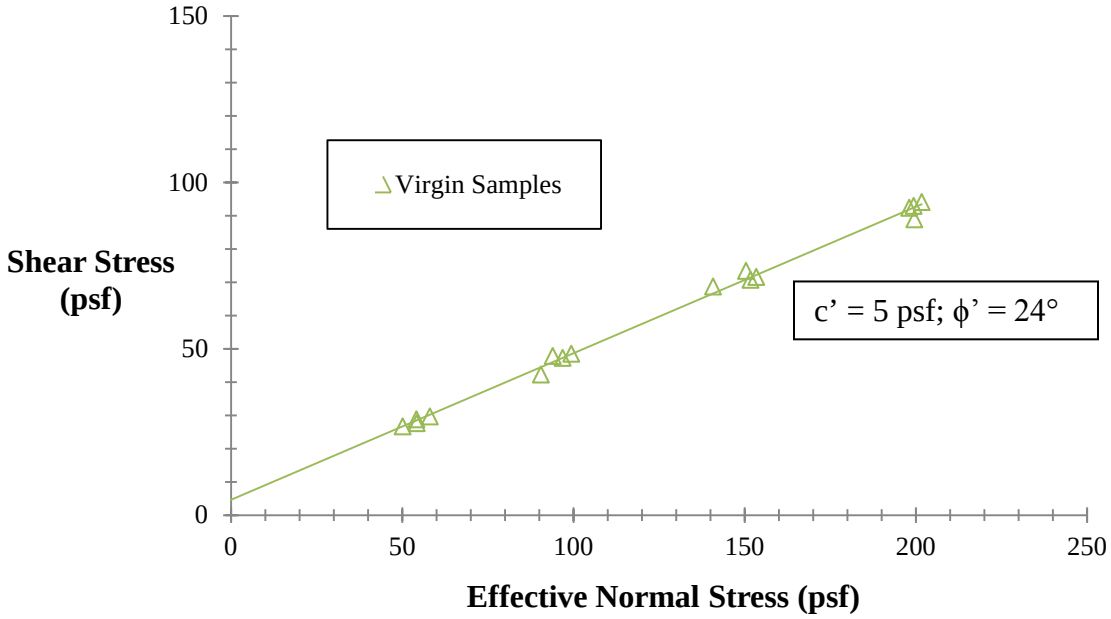

Figure 3.14: Interface shear strength envelope of virgin materials

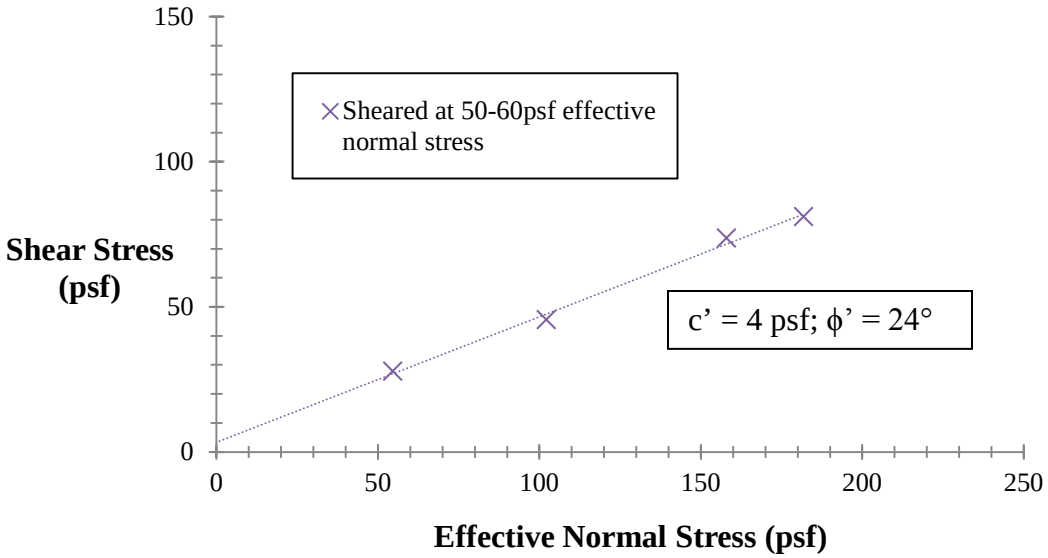

Figure 3.15: Available interface shear strength envelope of materials sheared at 50-60psf effective normal stress

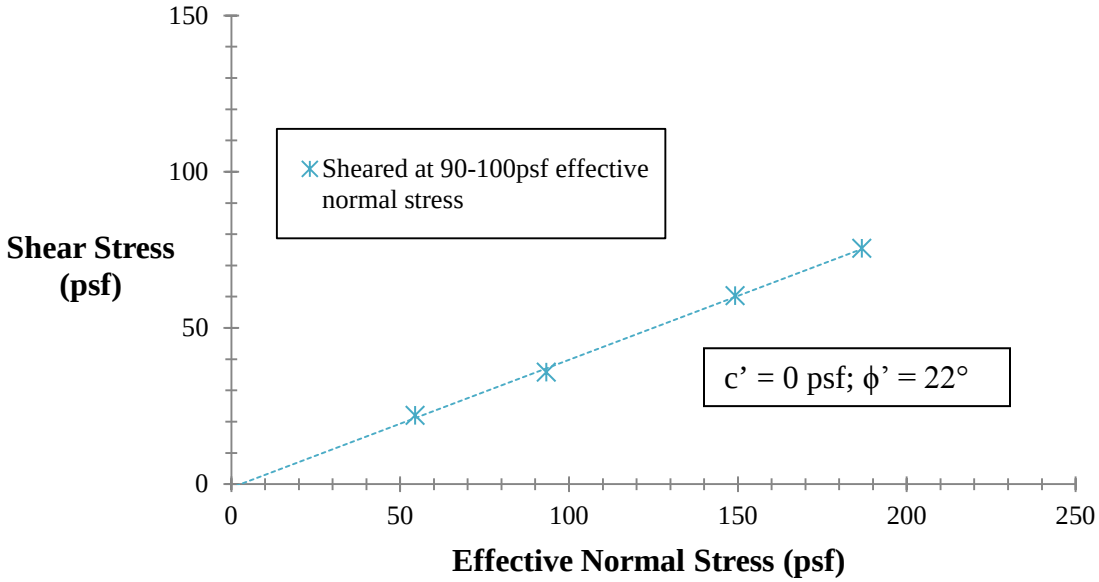

Figure 3.16: Available interface shear strength envelope of materials sheared at 90-100psf effective normal stress

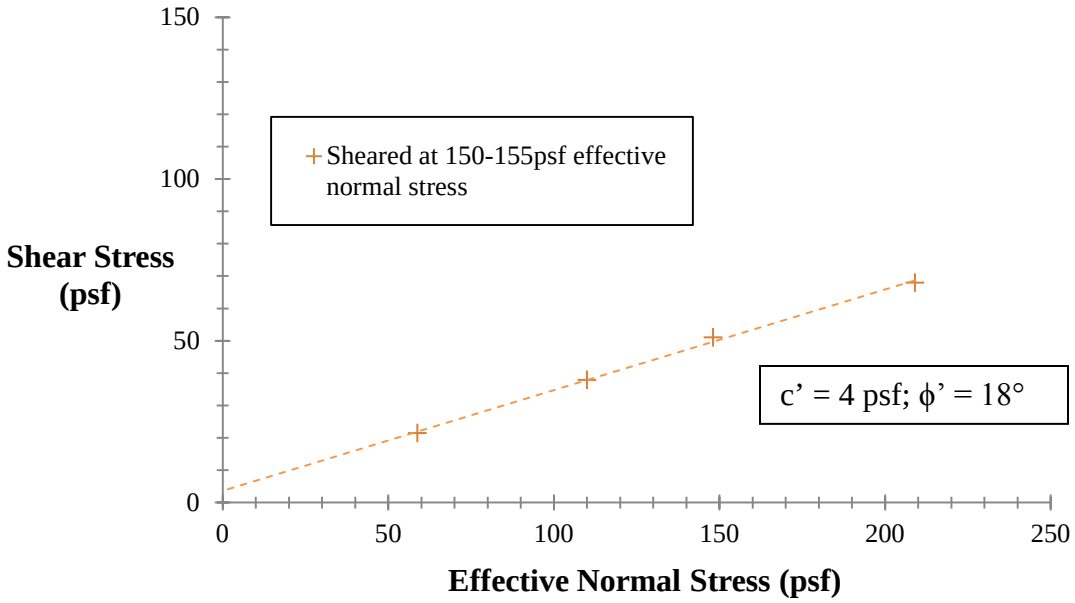

Figure 3.17: Available interface shear strength envelope of materials sheared at 150-155psf effective normal stress

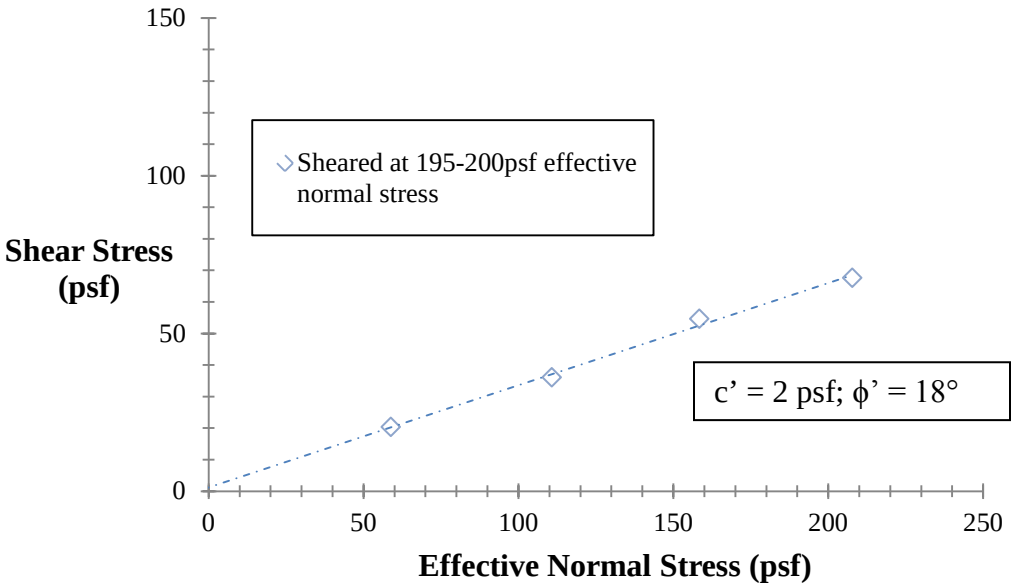

Figure 3.18: Available interface shear strength envelope of materials sheared at 195-200 psf effective normal stress

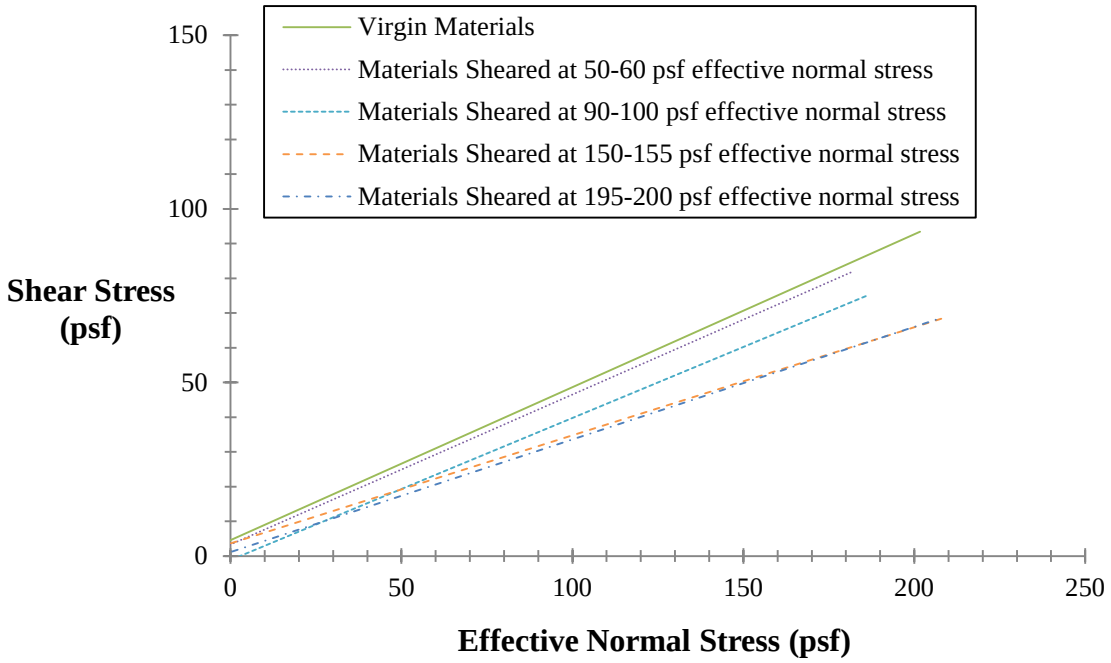

Figure 3.19: Interface shear strength envelopes for virgin materials and materials sheared at 50-60psf, 90-100psf, 150-155psf, and 195-200psf effective normal stress

Table 3.2: Apparent cohesion intercepts and frictions angles of interface shear strength envelopes

Sample Condition	**Interface Shear Strength Envelope**
Virgin	c' = 5 psf; ϕ' = 24°
Sheared at σ_n' = 50-60 psf	c' = 4 psf; ϕ' = 24°
Sheared at σ_n' = 90-100 psf	c' = 0 psf; ϕ' = 22°
Sheared at σ_n' = 150-155 psf	c' = 4 psf; ϕ' = 18°
Sheared at σ_n' = 195-200 psf	c' = 2 psf; ϕ' = 18°

3.4.5 Discussion

The SKAPS TN 270-2-6 / Poly-Flex 40-mil LLDPE textured geomembrane interface had strain softening behavior when sheared under 90 psf or greater effective

normal stress. This assumes similar behavior to previous research, where re-tested samples peak shear strength was approximately equal to the large displacement shear stress of the previous trial. Only the peak secant friction angle was recorded for each trial because rapid displacement after sliding commenced made direct measurement of post-peak interface shear strength difficult.

The change in available shear strength from the 1st trial to the 2nd depended on the normal stress at which the virgin materials were sheared, but not the effective normal stress at which the materials were re-tested (Figure 3.20). Virgin materials sheared at 90-100 psf effective normal stress had approximately 80% peak interface shear strength available at all effective normal stresses when re-tested. Materials previously sheared at 150 psf or greater had 70% of the peak interface shear strength available at all effective normal stresses when re-tested.

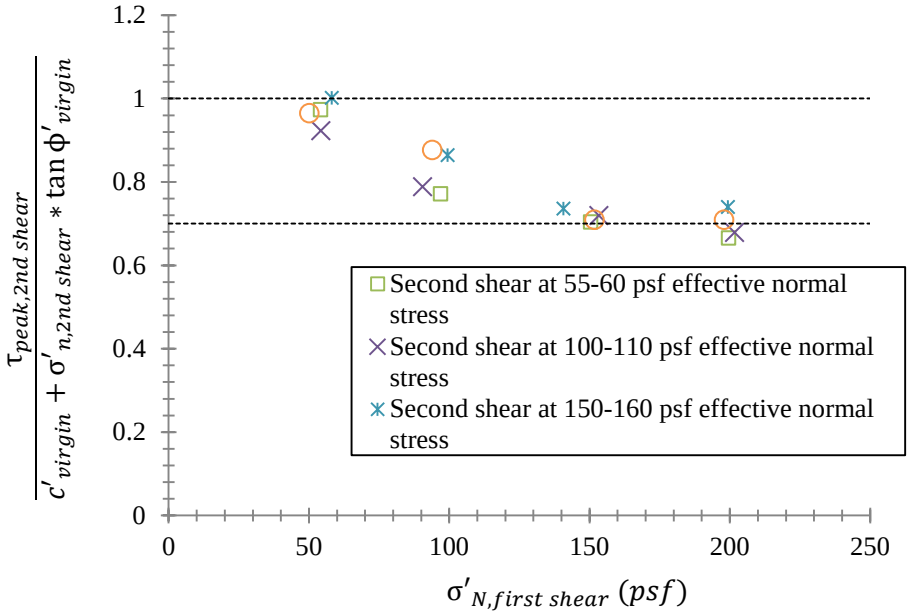

Figure 3.20: Ratio of peak shear stress measured in 2nd trial to peak shear stress predicted by virgin material shear strength envelope at the same effective normal stress as 2nd trial

This has several implications, considering landfill cover materials experience a range of effective normal stresses during construction and the design life of the facility. Large displacements during consruction will not reduce the available interface shear strength of geosynthetic landfill cover materials as long as the displacements occur at low effective normal stresses (such as the self weight of the geocomposite material). The lack of strain softening behavior at low normal stresses may also improve the long-term stability of the cover slope. In cases where cover materials displace down-slope, but remain intact, as the drainage layer fills and empties, the geocomposite/geomembrane interface would be expected to lose little shear strength if the displacement occurs at low effective normal stress.

From a forensic engineering perspective, the effective normal stress at the time of failure, and therefore the water pressure at failure, may be estimated by comparing the sheared (failed) materials' peak available shear strength to virgin materials' peak strength and considering the normal stress dependant strain softening behavior of the materials.

CHAPTER 4: HYDRAULIC MODELING

4.1 INTRODUCTION

In this chapter a simple hydrostatic example is presented to illustrate that defining equivalence between geocomposite and granular drainage layers using saturated transmissivity neglects the dramatically different storage capacities of the two drainage systems. A numerical model for confined flow in a geosynthetic drainage layer with a constrained outlet is also presented.

In "The Myth of Hydraulic Transmissivity Equivalancy Between Geosynthetic and Granular Liquid Collection Layers", Giroud et al. (2000) used analytical methods to demonstrate that for granular and geosynthetic drainage layers with the same confined, saturated transmissivity, the much thicker granular drainage layer will have a greater unconfined flow capacity. This thesis seeks to emphasize that even with confined flow there is an important difference between "equivalent" geosynthetic and granular drainage layers: storage capacity. Further, the relatively small storage capacity of geosynthetic drainage materials may lead to significant pore water pressures from modest rainfall events if there is constrained flow at the drainage layer outlet.

4.2 HYDROSTATIC ILLUSTRATIVE EXAMPLE

The example landfill cover presented in Chapter 1.2 (Figure 1.1) will be used in this section and throughout Chapter 4. The cover consists of 2 ft of cover soil and a geocomposite drainage layer overlying a composite hydraulic barrier layer made of a textured geomembrane and compacted clay. The slope is 90 ft long at an inclination of 3H:1V. If the geocomposite drainage layer is 250-mil thick and has a porosity of 0.8, the

entire length of the slope could be filled with 1.6 ft^3 of water (for a 1-ft unit width of the slope). If the slope were completely full under hydrostatic conditions, the pore pressure at the toe of the slope would be 1770 psf. Now consider the same slope, changing only the geosynthetic drainage layer to a 1-ft thick granular drainage layer. If the granular drainage layer contained the same 1.6 ft^3 of water that completely filled the geosynthetic drainage layer, there would be less than 1-ft of head above the hydraulic barrier layer at the toe of the slope, and the maximum pore water pressure at the drainage layer/geomembrane interface would be approximately 40 psf.

4.3 NUMERICAL MODEL OF CONFINED FLOW WITH A CONSTRAINED OUTLET

The model of confined flow presented in this chapter uses numerical methods to predict how water accumulation and water pressure in the drainage change over time. The model was developed for landfill covers systems with geocomposite drainage layers that daylight at the toe of the cover slope. The datum is placed at the drainage layer outlet (located at the toe of the slope), and it is assumed that water exiting the drainage system at the toe has zero total head.

The model is based on Darcy's Law:

$$q = k * i * A \qquad \text{Equation 4.1}$$

q is the volumetric flow rate through a permeable material, k is the material's hydraulic conductivity, i is the hydraulic gradient, and A is the cross-sectional area through which the water flows.

For the landfill cover system being evaluated, the hydraulic gradient (i) may be expressed as the total head loss (h) divided by the length of flow (L):

$$i = \frac{h}{L} \qquad \text{Equation 4.2}$$

Substituting Equation 4.2 into Equation 4.1 and solving for h gives an expression for the total head loss in the system:

$$h = \frac{q * L}{k * A} \qquad \text{Equation 4.3}$$

Transmissivity (θ) is defined as a material's hydraulic conductivity (k) times its thickness (T):

$$\theta = k * T \qquad \text{Equation 4.4}$$

For a 1-ft unit width of slope, Equations 4.3 and 4.4 may be combined and simplified to express the total head loss in the system in terms of transmissivity, volumetric flow rate, and length:

$$h = \frac{q * L}{\theta} \qquad \text{Equation 4.5}$$

The total head loss in the system (h) is equal to the sum of the head loss in the soil blockage (Δh_b), the head loss in the horizontal geosynthetic drainage material(Δh_{gc}), and the head loss in the inclined geosynthetic drainage material (Δh_h):

$$h = \Delta h_b + \Delta h_{gc} + \Delta h_h \qquad \text{Equation 4.6}$$

Further, the head loss in each component of the drainage system may be expressed using Darcy's Law:

$$\Delta h_b = \frac{q * L_b}{\theta_b} \qquad \text{Equation 4.7}$$

$$\Delta h_{gc} = \frac{q * L_{gc}}{\theta_{gc}} \qquad \text{Equation 4.8}$$

$$\Delta h_h = \frac{q * L_h}{\theta_h} \qquad \text{Equation 4.9}$$

L_b, L_{gc}, and L_h are the lengths of the soil blockage at the outlet, the horizontal geocomposite, and the inclined geocomposite respectively. θ_b, θ_{gc}, and θ_h are the transmissivities of the soil blockage at the outlet, the horizontal geocomposite, and the inclined geocomposite respectively. Substituting equations 4.7, 4.8, and 4.9 into 4.6 gives an expression for the total head loss of the system as the sum of the head loss in each component:

$$h = \frac{q * L_b}{\theta_b} + \frac{q * L_{gc}}{\theta_{gc}} + \frac{q * L_h}{\theta_h}$$ Equation 4.10

Equation 4.10 is then solved for q, the volumetric flow rate through the cover drainage system:

$$q = \frac{h}{\frac{L_b}{\theta_b} + \frac{L_{gc}}{\theta_{gc}} + \frac{L_h}{\theta_h}}$$ Equation 4.11

The volumetric flow rate into the drainage layer (I) is modeled by assuming some portion of the geocomposite drainage layer is left exposed during a rain event. The volumetric flow rate into the drainage layer depends on the rate of rainfall (r), the length of exposed geosynthetic drainage material (L_e), and the inclination of the exposed section of the drainage layer (β_e):

$$I = r * L_e * \cos \beta_e$$ Equation 4.12

Equation 4.12 gives the volumetric inflow rate for a 1 ft unit width of the slope.

The numerical model works by calculating the change in volume of water in the drainage layer (ΔV_w) based on the net volumetric flow rate into the drainage layer ($I - q$) over some amount of time Δt, using Equations 4.12 and 4.11 to calculate I and q, respectively:

$$\Delta V_w = (I - q)\Delta t$$ Equation 4.13

The change in the volume of water in the drainage layer can be used to calculate the change in total head in the system based on geometry and the porosity of the geocomposite drainage layer:

$$\Delta h = \frac{\Delta V_w}{n * T_{gc} * \sin\beta}$$ Equation 4.14

Finally, a new total head in the system ($h_{t+\Delta t}$) after time Δt has elapsed is calculated based on the previous total head in the system (h_t) and the change in total head (Δh):

$$h_{t+\Delta t} = h_t + \Delta h$$ Equation 4.15

An illustration of one time step is shown in Figure 4.1.

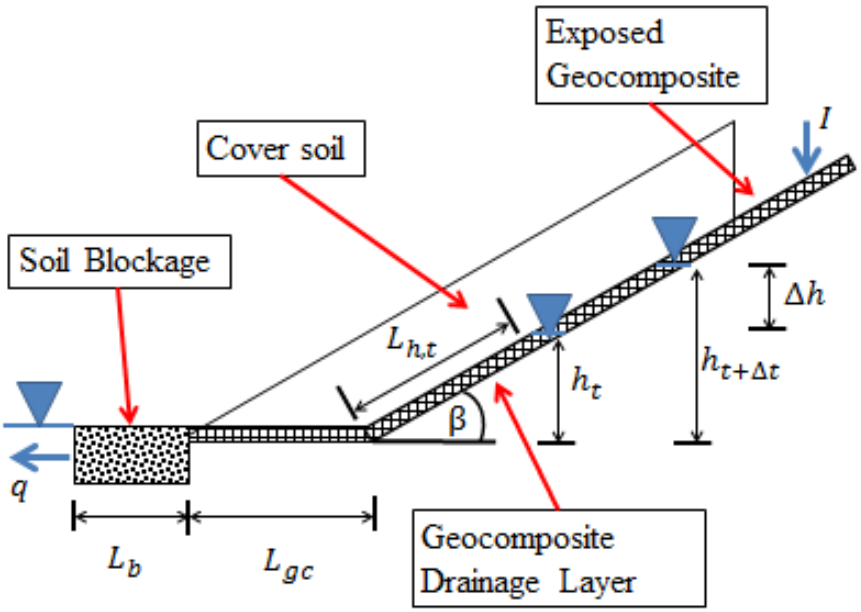

Figure 4.1: Cross-section of landfill cover system illustrating change in volume of water in drainage layer for one time-step in the numerical model

4.4 Verification of Numerical Model by Analytical Methods

A solution for the equilibrium total head loss in the system is derived analytically and used to verify the numerical calculations. At equilibrium, the change in total head (Δh) is equal to zero, which means the change in volume of water in the drainage layer (ΔV_w) is equal to zero. If the change in volume of water in the drainage layer is zero over some amount of time Δt, the net volumetric flow rate into the drainage layer ($I - q$) must be zero (Equation 4.13). In other words, at equilibrium the volumetric flow rate into the system (I) is equal to the volumetric flow rate out of the system (q). I may be substituted for q in Equation 4.10 to give an expression for the total head loss of the system at equilibrium:

$$h_{equilibrium} = \frac{I * L_b}{\theta_b} + \frac{I * L_{gc}}{\theta_{gc}} + \frac{I * L_h}{\theta_h}$$ Equation 4.16

At any given time the length of inclined geocomposite filled with water (L_h) may be related to the elevation of water and the inclination of the slope:

$$L_h = \frac{h}{\sin \beta}$$ Equation 4.17

Substituting Equation 4.17 into Equation 4.16 and solving for h gives an expression for the equilibrium total head loss in the system depending on the volumetric inflow rate and the geometry and transmissivity of the drainage system components:

$$h_{equilibrium} = \frac{I * \left(\frac{L_{gc}}{\theta_{gc}} + \frac{L_b}{\theta_b}\right)}{\left(1 - \frac{I}{\theta_{gc} \sin \beta}\right)}$$ Equation 4.18

4.5 EXAMPLE CALCULATIONS

Example calculations are presented for a precipitation event where 1 inch of rain falls in 8 hours over a slope with a 5-ft length of geosynthetic drainage layer exposed. Other variables describing the slope geometry and sample calculations are summarized in Table 4.1. The initial head in the system was assumed to be 0.001-ft and the time step increment used for the numerical analysis was 20 seconds.

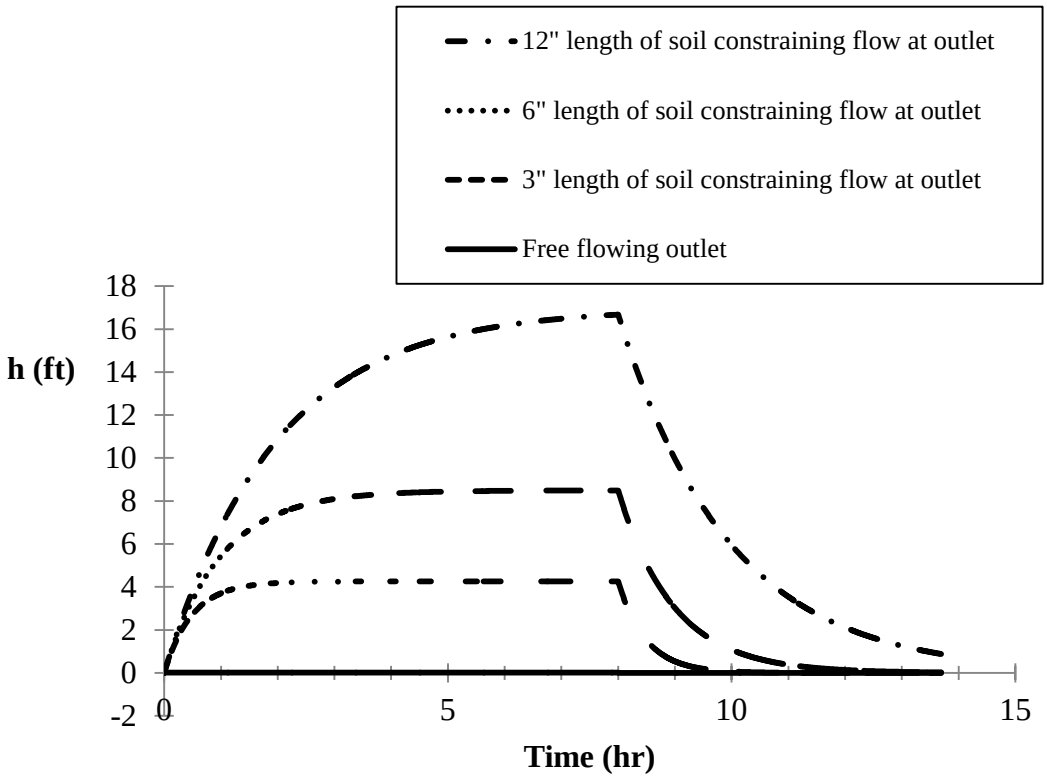

Figure 4.2: Parametric study varying the length of soil constraining flow at the outlet

Table 4.1: Properties used for numerical hydraulic model example calculations

Geocomposite Thickness	270-mil
Geocomposite Porosity	0.8
Geocomposite Transmissivity	$1.35*10^{-3} ft^2/s$ ($4.1*10^{-4}$ m^2/s)
Soil Blockage Thickness	3 in
Soil Blockage Hydraulic Conductivity	$4.0*10^{-5}$ in/s (10^{-4} cm/s)

Table 4.2: Analytical solutions for $h_{equilibrium}$

Length of soil blockage	$h_{equilibrium}$
0 in	0.02 ft
3 in	4.3 ft
6 in	8.5 ft
12 in	17.0 ft

4.6 DISCUSSION

The hydrostatic example demonstrates that a relatively small volume of water can create significant pore water pressures in geocomposite drainage layers due to the very small storage capacity of the geocomposite material. In the example calculations for the confined flow model, the cover drainage system performs adequately with no constraint at the outlet. The greatest build-up of total head in the drainage layer is 0.02 ft, or 1.3 psf of water pressure, when it is assumed that no soil blocks the toe outlet of the drainage layer. However, if water must pass through even modest lengths of soil having the permeability of silty sand to exit the system, water is shown to fill significant lengths of the drainage layer, creating significant pore water pressures at the geocomposite drainage material/textured geomembrane interface.

4.7 SUMMARY

A hydrostatic example was presented to demonstrate how dramatically different storage capacities of granular and geosynthetic drainage layers could lead elevated water pressures in geosynthetic drainage layers containing relatively small volumes of water.

Also, a numerical model was developed for confined flow in geocomposite drainage layers with constrained flow at the outlet, and the model was verified with an analytical solution for the equilibrium water elevation in the drainage layer. A parametric study demonstrating the numerical model was presented, showing that even a modest constraint at the drainage layer outlet may cause a significant build-up of water in a drainage system that performed adequately with no constraint at the outlet.

CHAPTER 5: STABILITY MODELING

5.1 INTRODUCTION

In this chapter a strain compatible slope stability model is developed and example stability solutions for a variety of pore water profiles are presented.

5.2 BACKGROUND

Landfill final cover stability has traditionally been analyzed with limit equilibrium methods by modeling the cover system as a finite slope (Soong and Koerner, 1996). In this type of analysis, the cover system is represented with an active wedge and a passive wedge, and possible seepage pressures acting on the wedges may be assumed (Figure 5.1). A limit equilibrium analysis of the cover slope stability includes several assumptions that may be unrealistic. Specifically, the limit equilibrium method assumes the active and passive wedges are rigid bodies with one shear strength envelope used to determine the maximum shear force mobilized on a potential slip surface. Displacements and strain softening may be accounted for implicitly in a limit equilibrium analysis, but a strain compatibility analysis is required to explicitly account for movement and strain-softening in the landfill cover slope.

A slope stability model for landfill cover systems satisfying force equilibrium and strain compatibility was developed by James Long, James Daly, and Robert Gilbert for the Office of Solid Waste Research at the University of Illinois in 1993. Their model calculated deflections and axial stresses in component of the landfill cover system. Strain softening of geosynthetic interfaces was accounted for, but pore water pressures in the slope were assumed. Further development yielded a similar model that also calculated pore water pressures in the slope, but free flowing conditions at the drainage layer outlet were assumed (Liu, 1998). The strain compatible stability model developed for this

research project builds on the previous research and includes two features that are different from the previous models:

- The strain softening of geosynthetic interfaces depends on the effective normal stress at the interface. Previous models included strain softening of geosynthetic interfaces, but the same shear stress – displacement relationship was used for all effective normal stresses.
- Pore water pressures are calculated assuming confined flow with a constrained drainage outlet. Previous models either required assumed pore water pressures or calculated water pressures assuming a free flowing outlet.

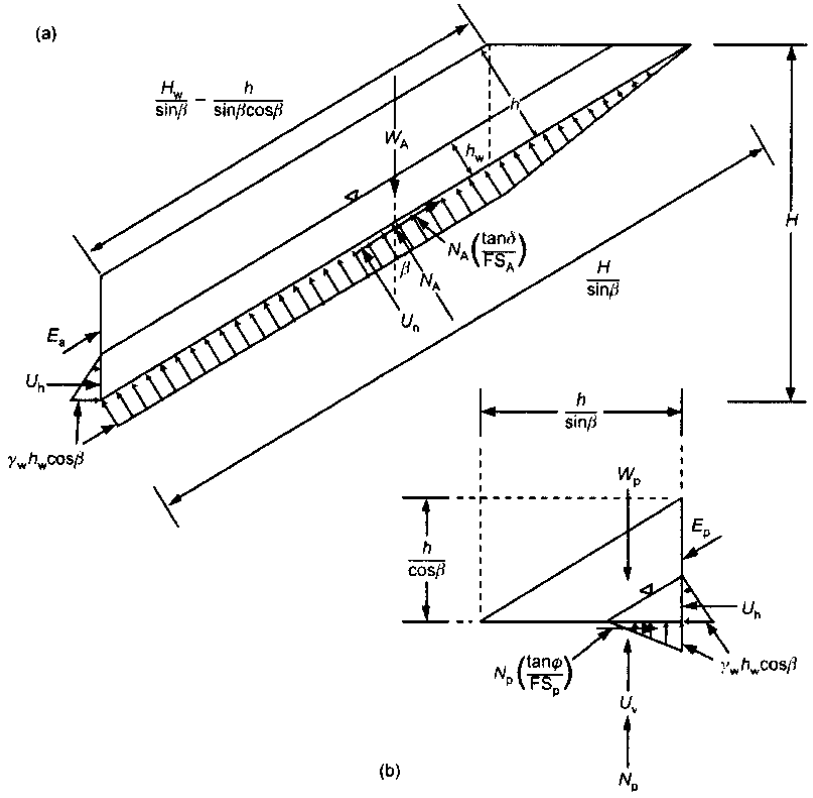

Figure 5.1: Limit equilibrium analysis of a landfill cover system using an (a) active wedge and (b) passive wedge to model the slope (Koerner and Soong, 2005)

5.3 STRAIN COMPATIBLE STABILITY MODEL

The strain compatible stability model presented in this chapter uses iterative numerical methods to calculate a slope stability solution that also satisfies strain compatibility. It was developed specifically to analyze landfill covers such as the examples presented in Chapter 2.3, which consist of protective soil and a geocomposite drainage layer overlying a composite hydraulic barrier layer. The geocomposite drainage layer and the overlying soil are modeled as a composite column that is divided into discrete elements. In tension, the axial stiffness of the composite column is due entirely to the geocomposite, and in compression the axial stiffness of the composite column is due entirely to the protective cover soil. In other words, it is assumed that the soil has zero tensile strength and the geocomposite has zero compressive strength. A buttress force at the toe of the slope is modeled as an elastic-plastic spring, with the maximum buttress force estimated using the geometry of the slope and the undrained shear strength of the protective cover soil. The geocomposite/textured geomembrane interface is modeled as a series of shear springs. Depending on the effective normal stress at the interface, the shear springs are either elastic-plastic or strain-softening. It is assumed that the textured geomembrane does not displace relative to the underlying compacted clay, and therefore that the geocomposite is the only layer of the cover system that can go into tension. Following geotechnical conventions, compression is adopted as positive throughout this chapter. All analyses are for a 1-ft unit width of slope.

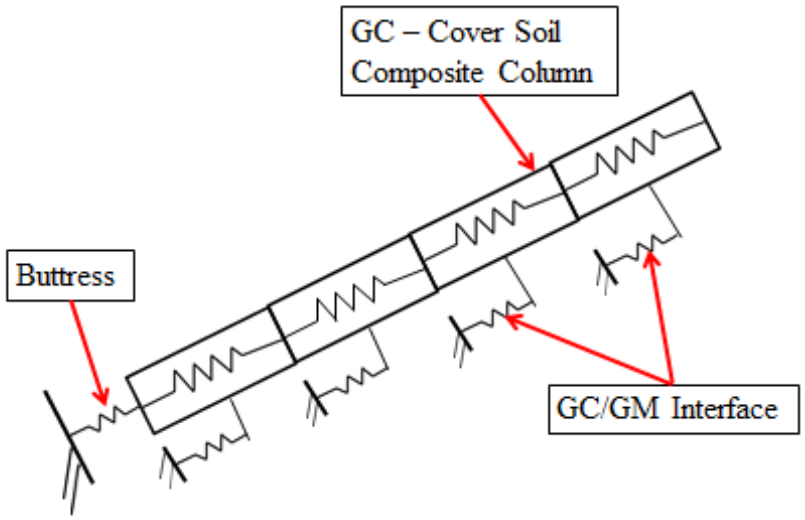

Figure 5.2: Strain compatible stability model of landfill cover system

5.3.1 Strain Compatible Force Equilibirum of ith element

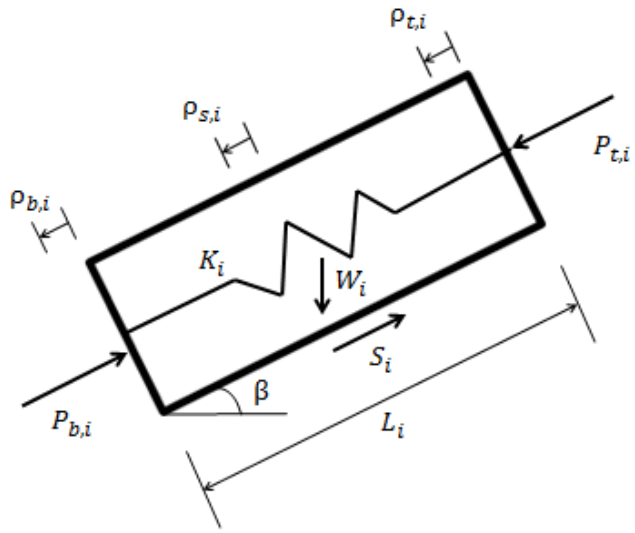

Figure 5.3: ith element of the composite column

For the landfill cover slope to be at equilibrium, each element of the composite column must be at equilibrium:

$$P_{b,i} + S_i - W_i \sin\beta - P_{t,i} = 0 \qquad \text{Equation 5.1}$$

Equation 5.1 must be true to satisfy force equilibrium in the direction of the slope inclination for element *i*. The displacement and deformation of the element must also be evaluated with respect to the axial stiffness of the composite column and the shear stiffness of the interface:

$$P_{avg,i} = \frac{P_{b,i} + P_{t,i}}{2} \qquad \text{Equation 5.2}$$

$$\Delta L_i = \frac{P_{avg,i}}{K_i} \qquad \text{Equation 5.3}$$

$$\rho_{t,i} = \rho_{b,i} + \Delta L_i \qquad \text{Equation 5.4}$$

$$\rho_{s,i} = \frac{\rho_{b,i} + \rho_{t,i}}{2} \qquad \text{Equation 5.5}$$

$$S_i = f_s * L_i \qquad \text{Equation 5.6}$$

Equations 5.2, 5.3, 5.4, 5.5, and 5.6 must all be true to satisfy strain compatibility. $P_{b,i}$ and $P_{t,i}$ are the forces acting on the bottom and top of the element, respectively, W_i is the weight of element *i*, and S_i is the interface shear force acting on the element *i*. L_i is the length of element *i*, ΔL_i is the change in length, and K_i is the axial stiffness of the element. $\rho_{b,i}$, $\rho_{t,i}$, and $\rho_{s,i}$ are the down-slope displacements of the bottom, top, and side of the element, respectively.

5.3.2 Geocomposite/Geomembrane Interface Shear Force

As shown in Equation 5.6, the geocomposite/geomembrane interface shear force (S_i) acting on element *i* depends on the shear stress developed at the interface ($f_{s,i}$) and the area over which the shear stress acts ($L_i * 1$). The interface shear stress developed ($f_{s,i}$) is a function of the average displacement of the element ($\rho_{s,i}$) and the maximum interface shear stress that may be developed ($f_{s,max,i}$). $f_{s,max,i}$ is defined as the shear strength envelope for the geocomposite/geomembrane interface and depends on the effective normal stress acting at the interface (Equation 5.7). The relationship between displacement (ρ_s) and the interface shear stress developed relative to the maximum interface shear stress is known is a "t-z" curve (Figure 5.4).

If the average pore water pressure acting on an element is equal to or greater than the total normal stress, zero shear stress is developed at the interface.

$$f_{s,max,i} = c' + \sigma'_N * \tan\phi' \qquad \text{Equation 5.7}$$

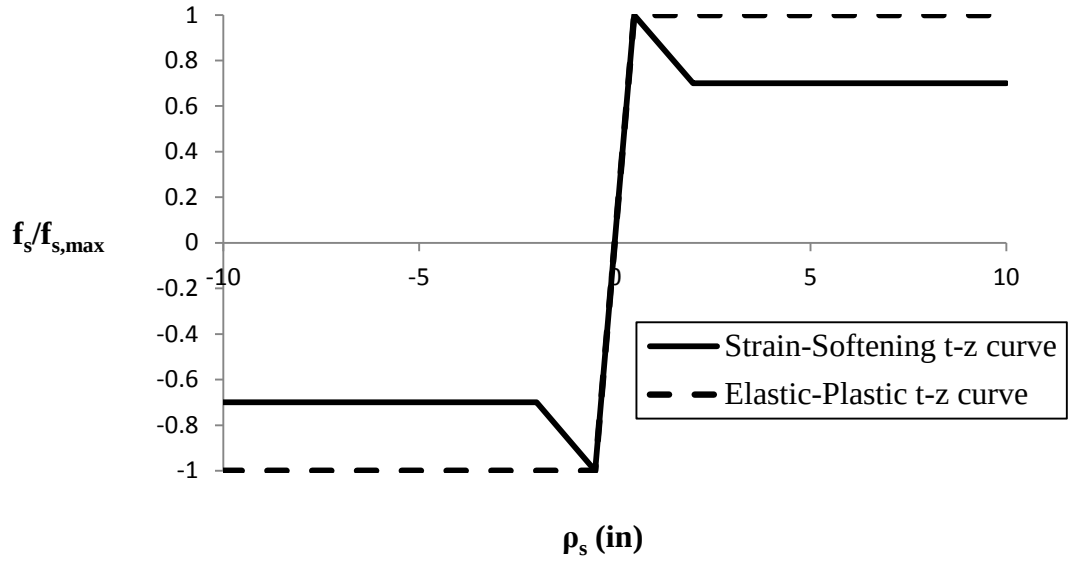

Figure 5.4: "t-z" curves for the geocomposite drainage material/textured geomembrane interface

The model uses the elastic-plastic “t-z” curve for elements with low effective normal stress at the interface and the strain-softening “t-z” curve for elements with high effective normal stress at the interface. Based on the results in Chapter 3, 100 psf is used as the threshold effective normal stress, above which the geocomposite/geomembrane interface is strain softening. Figure 5.5 expresses this graphically, where $f_{s,ld}$ is the shear stress mobilized at large displacements.

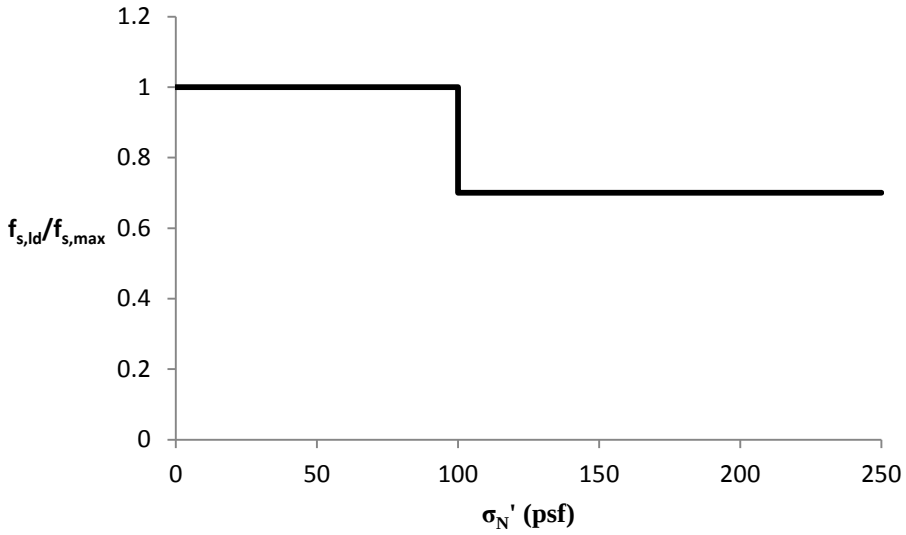

Figure 5.5: Idealized effective normal stress dependent strain-softening of geocomposite drainage material/textured geomembrane interface

5.3.3 Buttress Force

The buttress force mobilized at the toe of the slope is modeled as an elastic-plastic spring, and the relationship between displacement and force at the toe of the slope is called a "Q-z" curve. Q_{max} is the maximum buttress force that may be mobilized at the toe of the slope and is estimated using the geometry of the slope and the undrained shear strength of the protective cover soil.

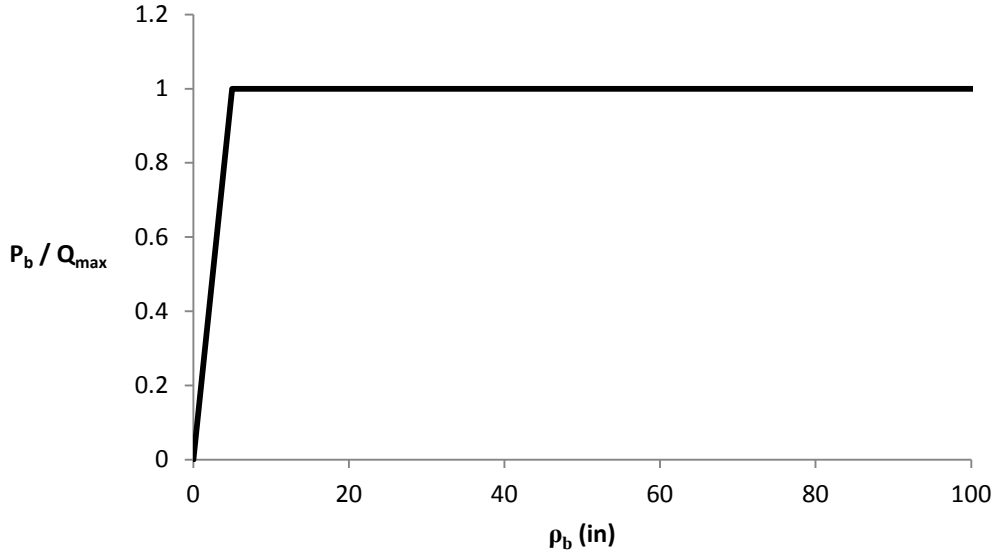

Figure 5.6: "Q-z" curve used to determine P_b at the toe of the slope

5.3.4 Solution Procedure

The model begins by iteratively calculating a strain compatible stability solution for the bottommost element of the composite column. The solution procedure for the first element is as follows:

1. Assume ρ_b
2. Calculate P_b using the "Q-z" curve
3. Assume P_t
4. Calculate P_{avg} with equation 5.2
5. Calculate ΔL with equation 5.3
6. Calculate ρ_t with equation 5.4
7. Calculate ρ_s with equation 5.5
8. Calculate S using equation 5.6 and the "t-z" curve
9. Calculate P_t with equation 5.1

Steps 3 through 9 are repeated until P_t assumed converges with P_t calculated. After convergence for element *i*, the same procedure is repeated for element $i + 1$, the next element up the slope. The model works its way up the slope by recognizing that the displacement and force at the bottom of an element are equal to the displacement and force at the top of the adjacent element down-slope (Equations 5.8 and 5.9). Each assumed displacement at the toe (ρ_b of the bottommost element, step 1) has a unique strain compatible stability solution for the slope, with unique boundary conditions ρ_t and P_t at the uppermost element. Different toe displacements may be selected to achieve a desired force or displacement boundary condition at the top of the composite column.

$$\rho_{t,i} = \rho_{b,i+1} \qquad \text{Equation 5.8}$$

$$P_{t,i} = P_{t,i+1} \qquad \text{Equation 5.9}$$

5.3.5 Verification

Two example solutions are presented to demonstrate that the strain compatible stability model functions properly. The example solutions are selected because they have analytical solutions and test various aspects of the stability model.

5.3.5.1 Infinite Slope Analysis

In an infinite slope analysis, the shear force (*S*) required to hold a length *l* of slope in place depends on the unit weight of the soil (γ), the depth to the slip surface (z), and the inclination of the slope (β):

$$S = \gamma * l * z * \cos\beta * \sin\beta$$ Equation 5.10

In the case of a 90 ft long 3H:1V cover slope with a 2 ft thickness of protective soil above the geocomposite drainage layer, 7,115 lbs of shear force at the geocomposite/textured geomembrane interface hold the slope in place. If the interface shear strength envelope has an apparent cohesion intercept of 9 psf and a friction angle of 27°, the maximum shear force that may be mobilized at the interface is 12,274 lbs, meaning 58% of the maximum shear force is mobilized. According to the assumed shear stress-displacement relationship (Figure 5.4), mobilized shear stress increases linearly from 0 to 100% of the maximum in 0.5 inches of displacement, so 0.58 * 0.5 = 0.290 inches of displacement are required to mobilize the shear force that holds the slope in place.

The model calculates an infinite slope-type solution with zero buttress force at the toe and a boundary condition of zero force acting on top of the uppermost element. The model solution agrees with the analytical infinitely slope analysis: the slope displaces 0.29 inches at all points along the interface, and there is zero axial force throughout the full length of the slope (Figures 5.7 and 5.8).

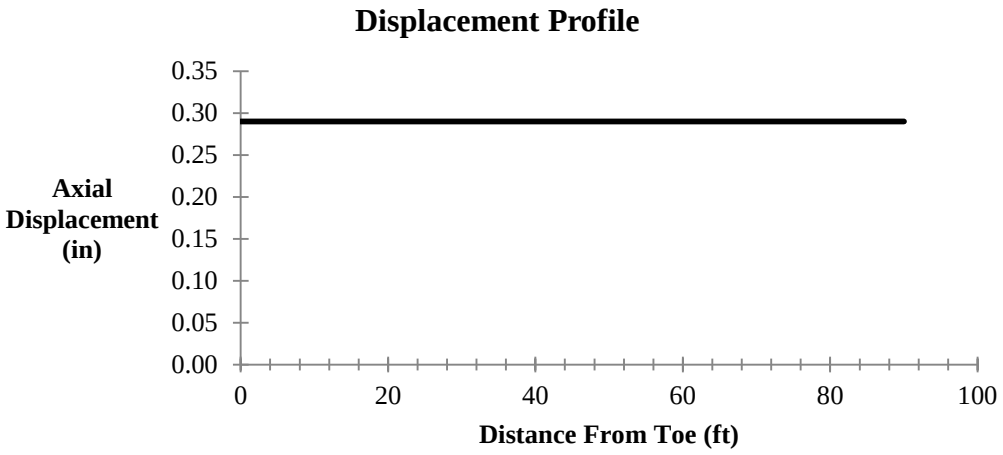

Figure 5.7: Displacement profile, infinite slope verification analysis

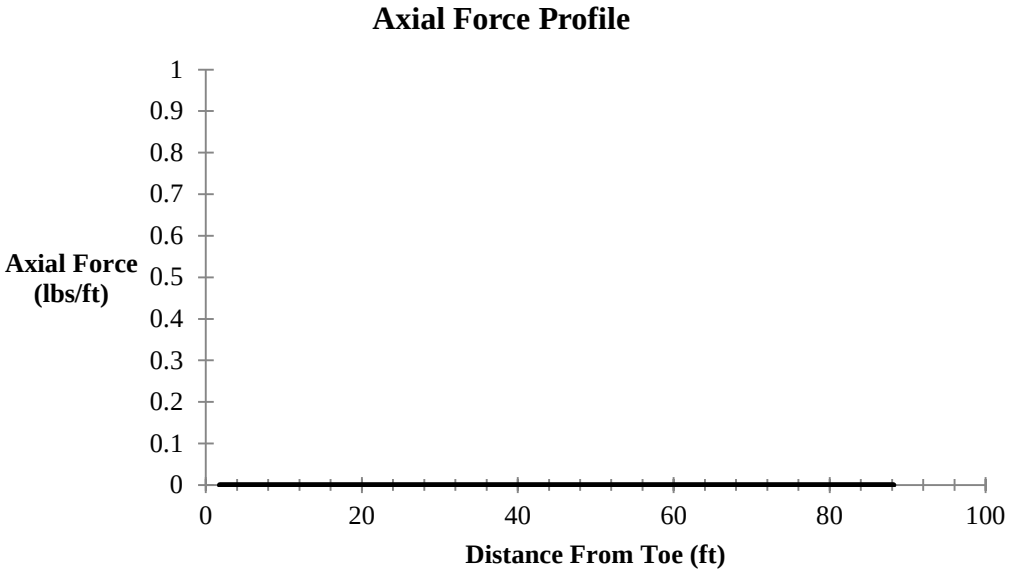

Figure 5.8: Profile of axial force per 1' unit width of slope, infinite slope verification analysis

5.3.5.2 Composite Column in Compression from Self-Weight

The case of a column of soil deforming under its own weight is presented to demonstrate that the numerical model properly accounts for the axial properties of the cover system components.

The change in length of a column (ΔL) is related to the force acting on the column (F), the original length of the column (L), the modulus of elasticity (E), and the cross sectional area of the column (A):

$$\Delta L = \frac{F * L}{A * E}$$

Equation 5.11

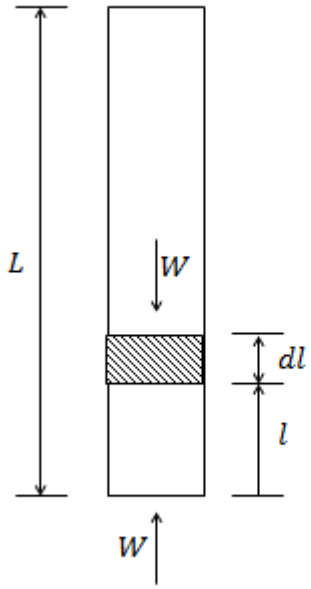

Figure 5.9: Diagram of vertical column of soil

In the case of a soil column deflecting under its own weight (W), the axial force depends on location (l) and ranges from the full weight of the column at the base to zero at the top:

$$F = W\left(\frac{L-l}{L}\right) \qquad \text{Equation 5.12}$$

The change in length of an element at location l can be evaluated by substituting Equation 5.12 into Equation 5.11:

$$\Delta dl = \frac{W}{EA}\left(\frac{L-l}{L}\right) dl \qquad \text{Equation 5.13}$$

The total change in length of the soil column (ΔL) may be calculated by integrating the changes in length of the elements (Δdl) over the full length of the column:

$$\Delta L = \int_0^L \frac{W}{EA}\left(\frac{L-l}{L}\right) dl \qquad \text{Equation 5.14}$$

Equation 5.14 is evaluated to give the analytical solution for a column deflecting under its own weight:

$$\Delta L = \frac{-WL}{2EA} \qquad \text{Equation 5.15}$$

In the case of a 90 ft long, 2 ft x 1ft column of soil with unit weight 125 pcf and modulus of elasticity 150 psi, the analytically calculated change in length of the soil column is 23.4 ft.

To evaluate the case of a vertical column of soil, the model considers zero shear force at the interface and a buttress force equal to the full weight of the soil column. As shown in Figures 5.10 and 5.11, the solution calculated with the numerical model agrees with the analytical solution. The maximum deflection is located at the top of the uppermost element and has a magnitude of 281 inches, or 23.4 ft.

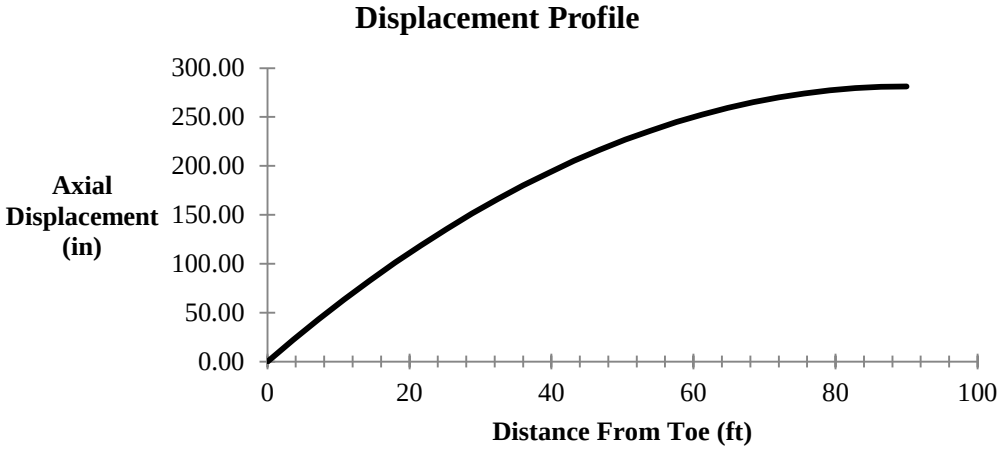

Figure 5.10: Displacement profile of vertical column of soil

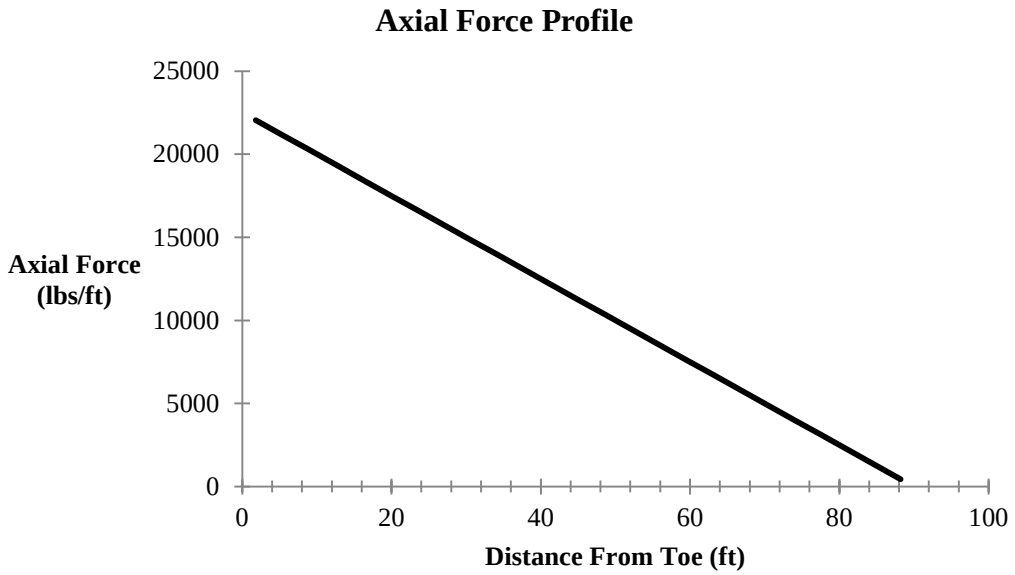

Figure 5.11: Axial force distribution for a verical column of soil

5.4 EXAMPLE STABILITY ANALYSES

The solutions presented in this section are for a 90-ft long 3H:1V cover slope with a 2-ft thick soil protection layer over the geocomposite drainage layer (Figure 5.7). The geocomposite drainage layer sits above a textured geomembrane. The 90-ft long slope was divided into 25 elements for the analysis. Important properties for the slope materials and the geocomposite/geomembrane interface are reported in Table 5.1. Each solution was calculated to satisfy the boundary condition $\rho_t = 0$ for the uppermost element within a tolerance of +/- 0.25 inches. A zero displacement boundary condition for the top of the uppermost element was selected to model a geocomposite drainage layer that is anchored at the crest of the slope.

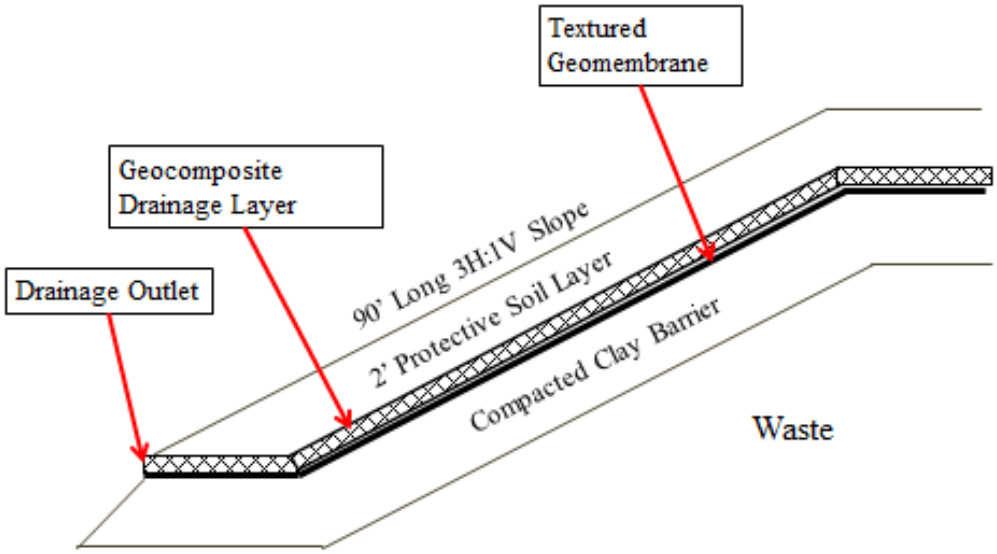

Figure 5.12: Cross-section of cover slope used for strain compatible stability analyses of cover slope (not to scale)

Six example solutions are presented. The geometry and material properties of the cover slope system are the same for every solution; only the pore water pressures in the geocomposite drainage layer vary.

Solutions for three assumed uniform pore water pressure profiles are presented: 0 psf water pressure along the full length of the slope, 100 psf water pressure along the full length of the slope, and 200 psf pore water pressure along the full length of the slope. The uniform pore water pressure examples are presented to illustrate how the geocomposite/geomembrane interface is modeled as strain-softening at high effective normal stresses but not at low effective normal stresses, and also to demonstrate that the cover system experiences larger deflections and axial forces when the effective normal

stress (and therefore the available interface shear strength) at the geocomposite/geomembrane interface decreases.

Next, a solution is presented for a cover slope with uniform pore water pressure in a portion of the drainage layer and zero pore water pressure in the rest of the drainage layer. This example solution demonstrates that the strain compatible stability model is capable of analyzing a slope with pore pressures similar to those that may be assumed for a limit equilibrium analysis.

Finally, two solutions are presented for cases where the pore water pressures in the geosynthetic drainage layer are calculated using the numerical model for confined flow with a constrained outlet. The rain event, length of exposed drainage material, and assumed soil blockage at the toe outlet used to calculate the pore pressures in the drainage layer are explained before each of the stability solutions is presented.

Table 5.1: Material and interface properties used for example slope stability calculations

$K_{i,tension}$	50.9 lbs/in
$K_{i,compression}$	1000 lbs/in
Cover Soil Unit Weight	125 pcf
c’ (interface)	9 psf
ϕ’ (interface)	27°

5.4.1 Uniform Water Pressure at the Interface

5.4.1.1 Zero Pore Water Pressure

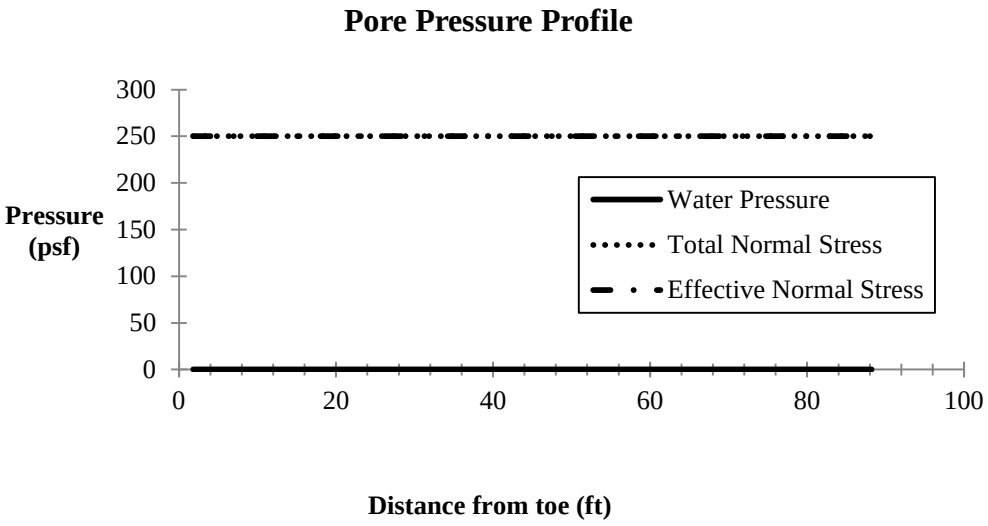

Figure 5.13: Pore pressure profile, zero water pressure at interface

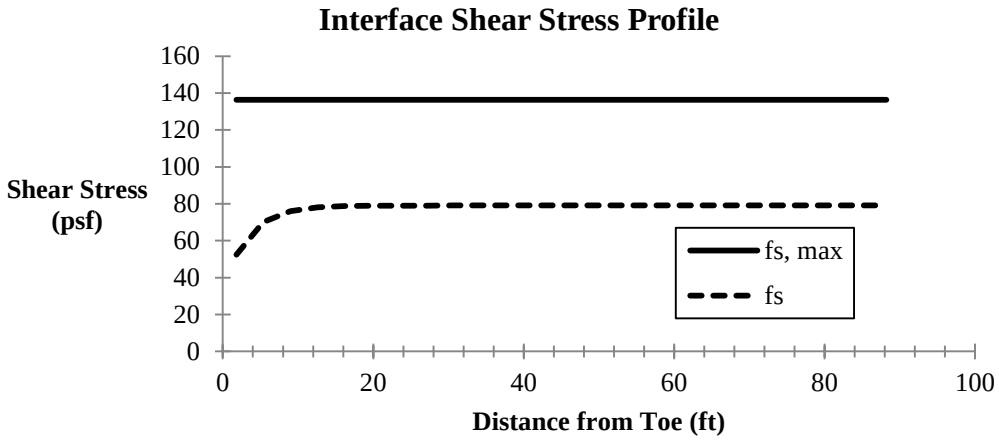

Figure 5.14: Shear stress profile, zero water pressure at interface

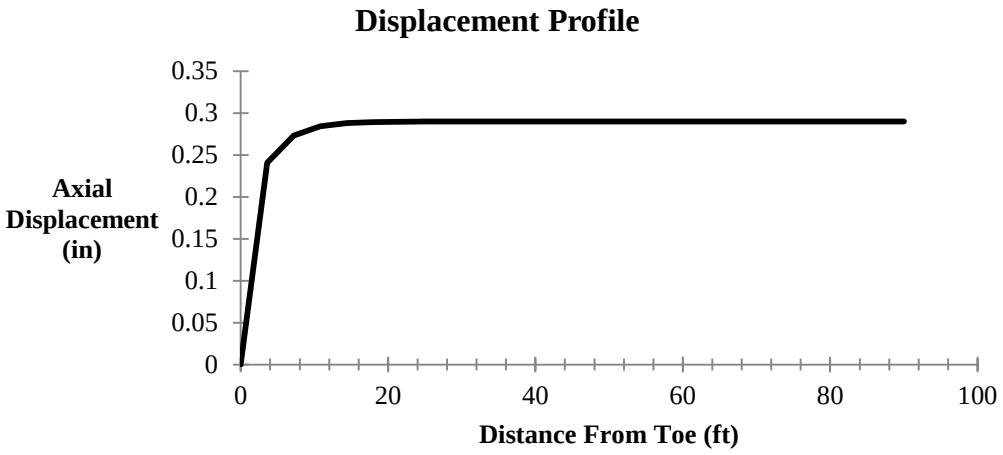

Figure 5.15: Displacement profile, zero water pressure at interface

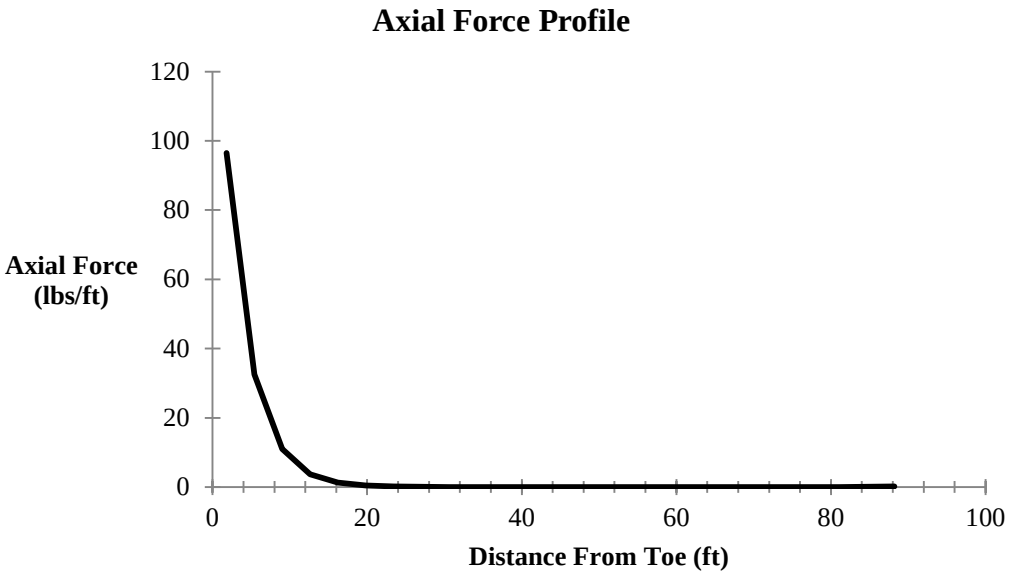

Figure 5.16: Profile of axial force per 1’ width of slope, zero water pressure at interface

5.4.1.2 100 psf Uniform Pore Water Pressure

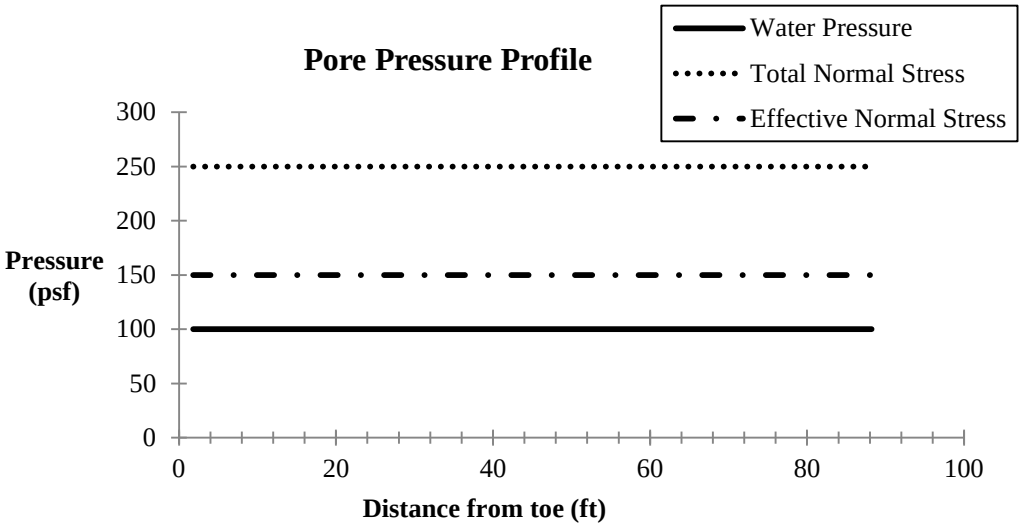

Figure 5.17: Pore pressure profile, 100 psf uniform water pressure at interface

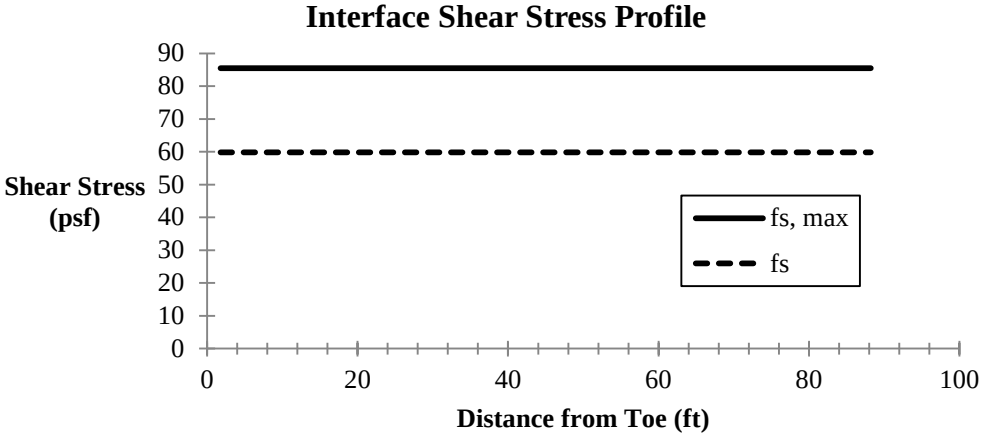

Figure 5.18: Interface shear stress profile, 100 psf uniform water pressure at interface

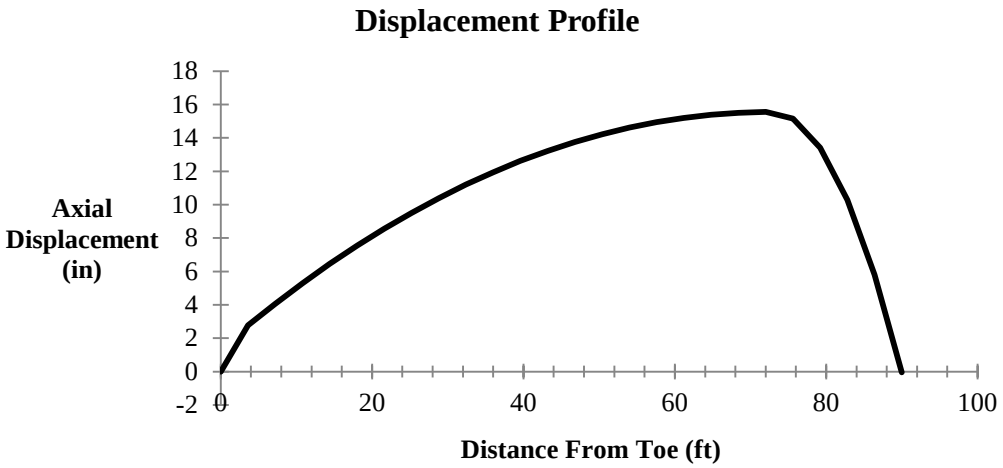

Figure 5.19: Displacement profile, 100 psf uniform water pressure at interface

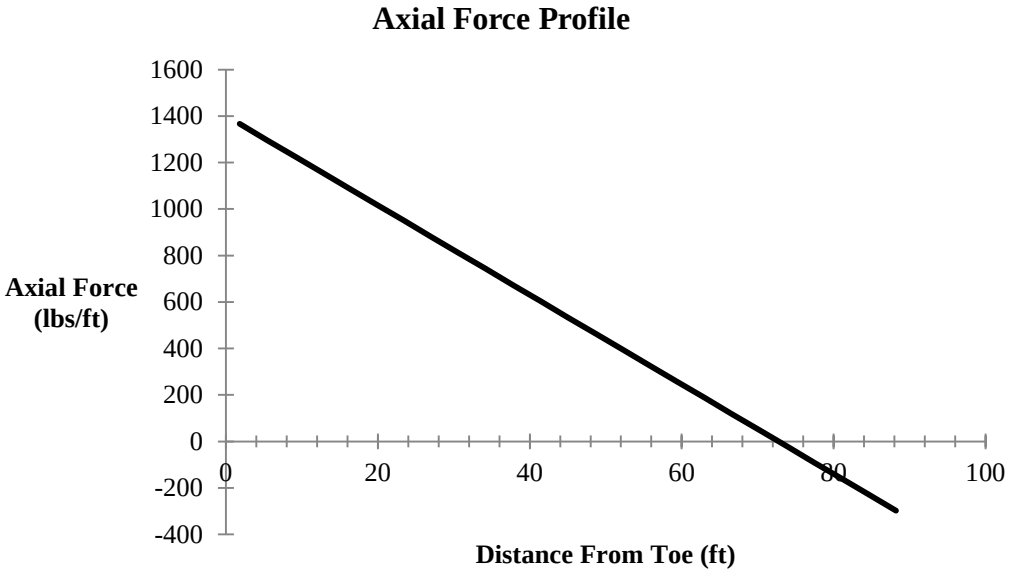

Figure 5.20: Profile of axial force per 1' unit width of slope, 100 psf uniform water pressure at interface

5.4.1.3 200 psf Uniform Pore Water Pressure

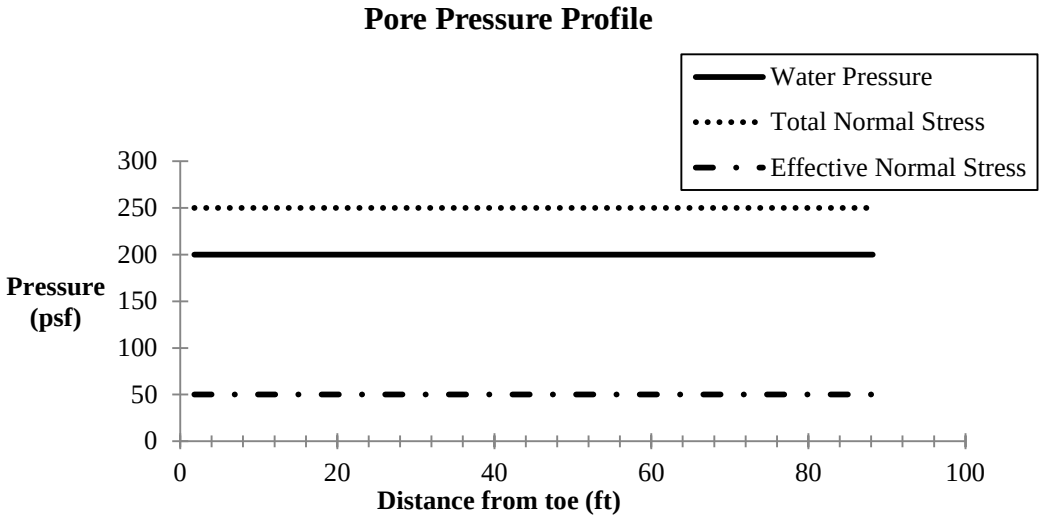

Figure 5.21: Pore pressure profile, 200 psf uniform water pressure at interface

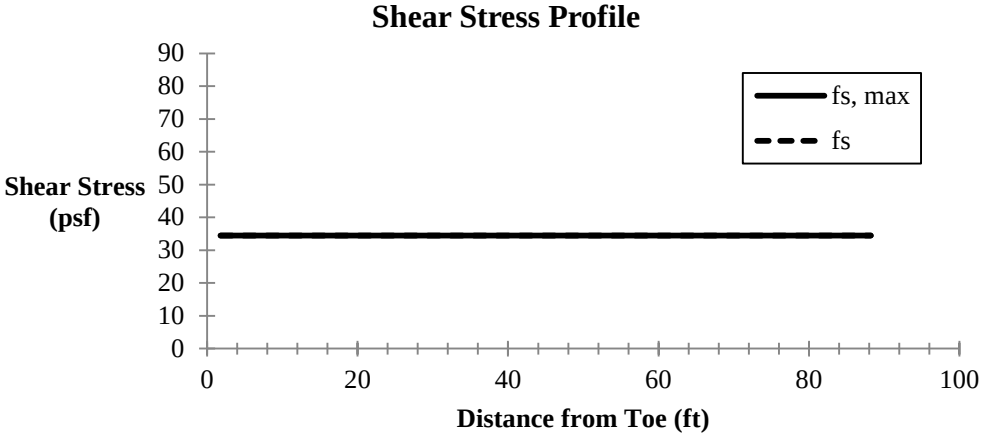

Figure 5.22: Shear stress profile, 200 psf uniform water pressure at interface

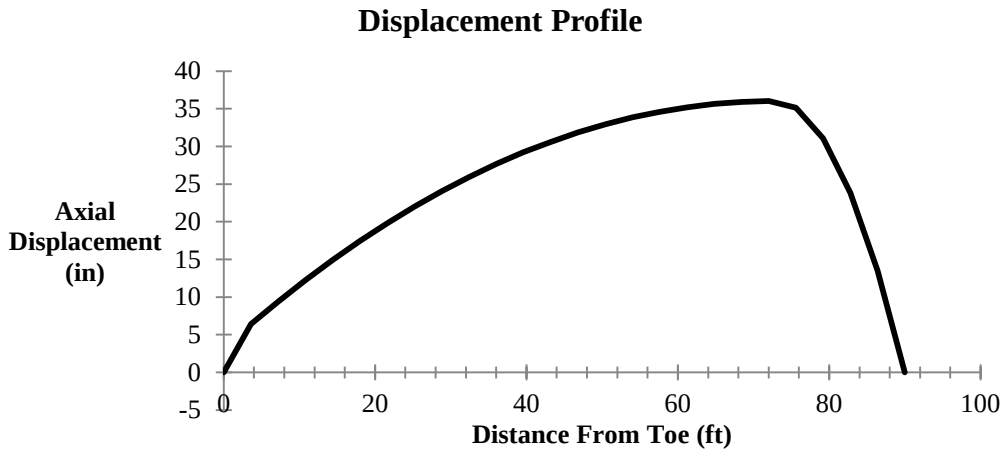

Figure 5.23: Displacement profile, 200 psf uniform water pressure at interface

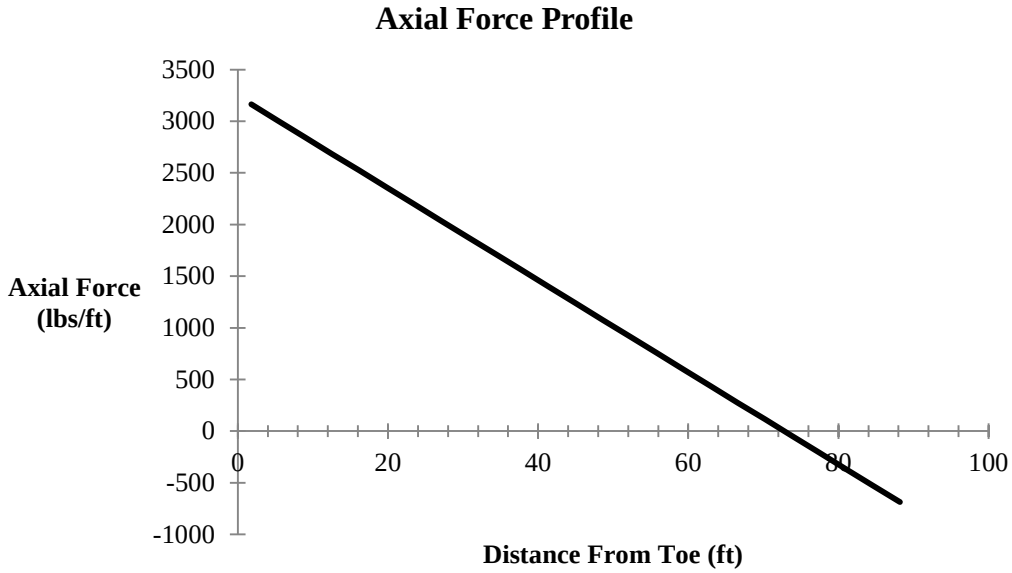

Figure 5.24: Profile of axial force per 1' unit width of slope, 200 psf uniform water pressure at interface

5.4.2 Uniform Water Pressure on a Portion of the Interface

5.4.2.1 150 psf on the Bottom 50-ft of the Slope

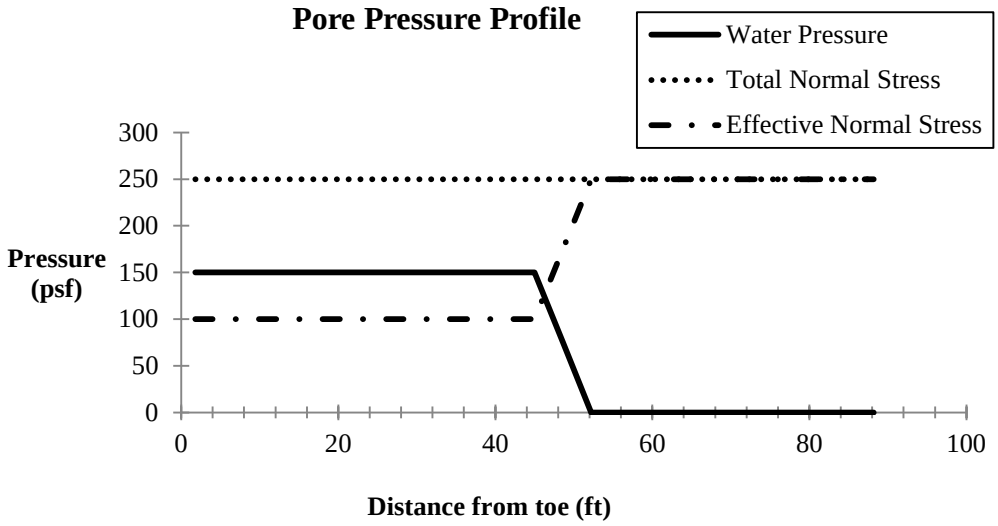

Figure 5.25 Pore pressure profile, 150 psf water pressure on bottom 50’ of slope

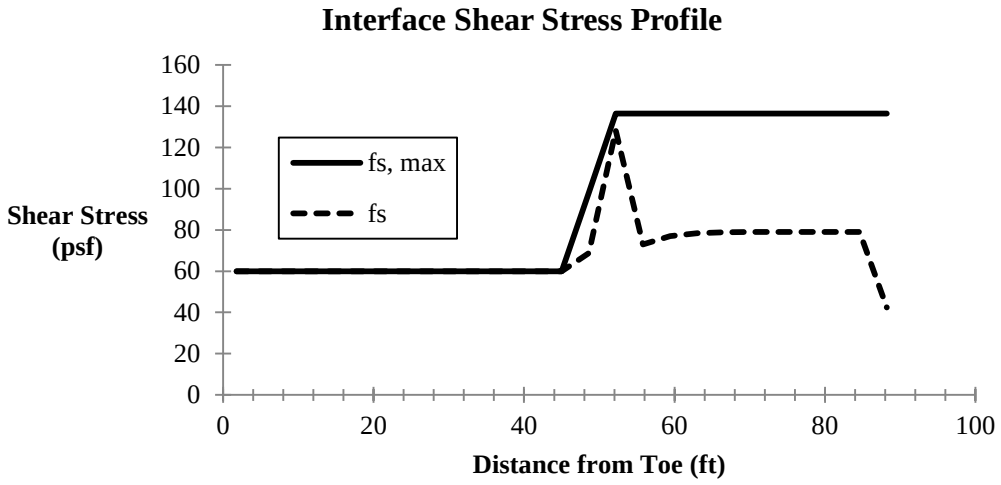

Figure 5.26: Interface shear stress profile, 150 psf water pressure on bottom 50’ of slope

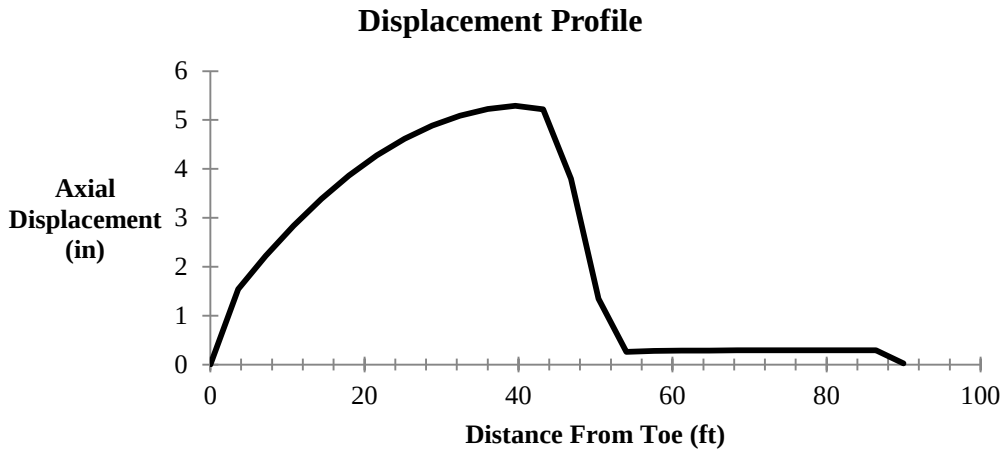

Figure 5.27: Displacement profile, 150 psf water pressure on bottom 50’ of slope

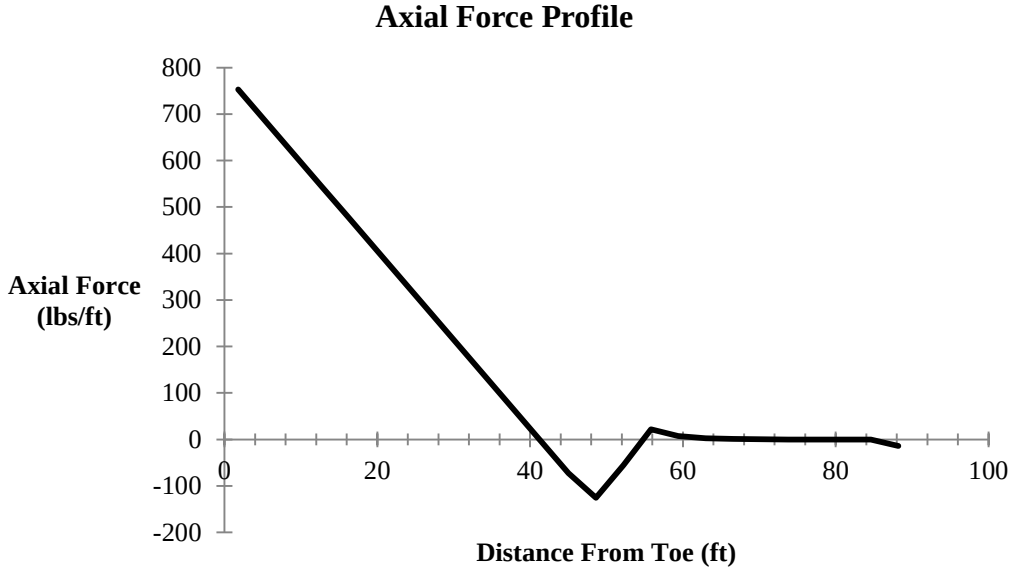

Figure 5.28: Profile of axial force per 1’ unit width of slope, 150 psf water pressure on bottom 50’ of slope

5.4.3 Calculated Pore Water Pressures

5.4.3.1 Case of 27’ of geocomposite containing water, h_{max} = 8.5’

In this example, 1 inch of rain falls in 8 hours, and 5’ of geocomposite drainage material are left exposed and open to the infiltrating water. The constraint to flow at the

drainage layer outlet is modeled with a block of soil 3 inches thick and 6 inches long, having the hydraulic conductivity of silty sand, $4*10^{-5}$ in/s ($1*10^{-4}$ cm/s). The pore water pressure profile is calculated for the case during the rain event when the water pressures in the drainage layer are greatest. In this case, pore water pressures are greatest when the water filling the drainage layer has come to equilibrium at an elevation of 8.5 ft, filling a 27-ft length of the drainage layer in the slope.

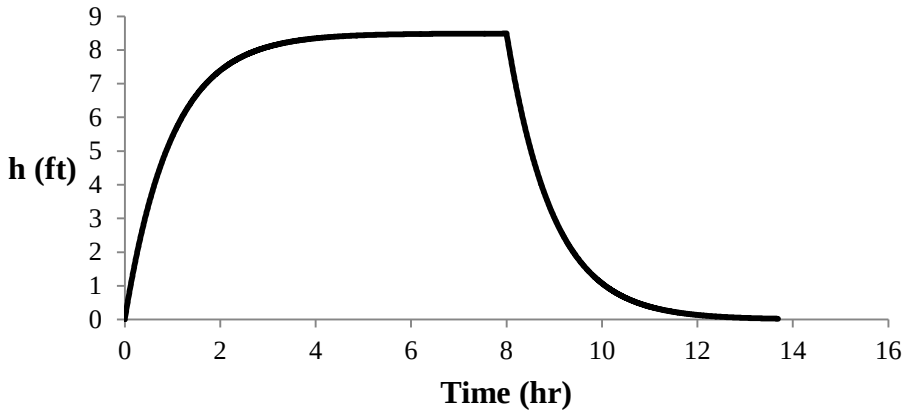

Figure 5.29: Change in water elevation in geocomposite during rain event, h_{max} = 8.5’

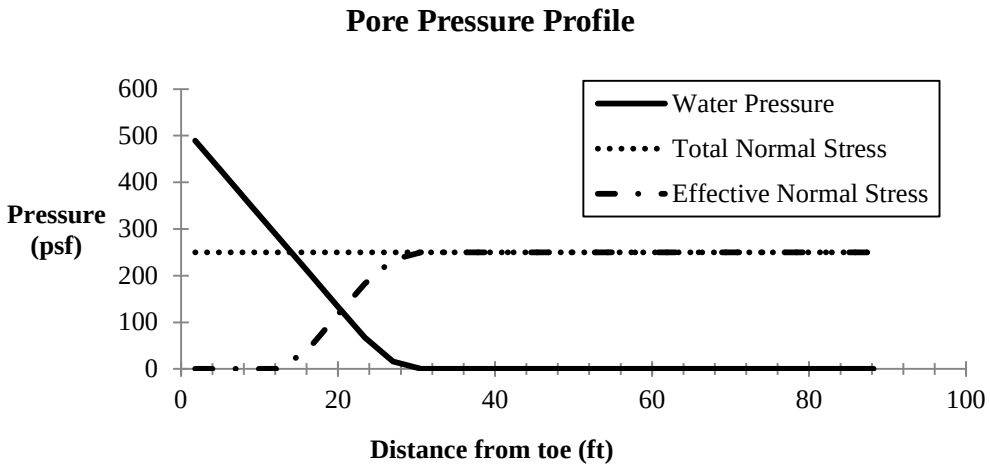

Figure 5.30: Pore water pressure profile, h_{max} = 8.5’

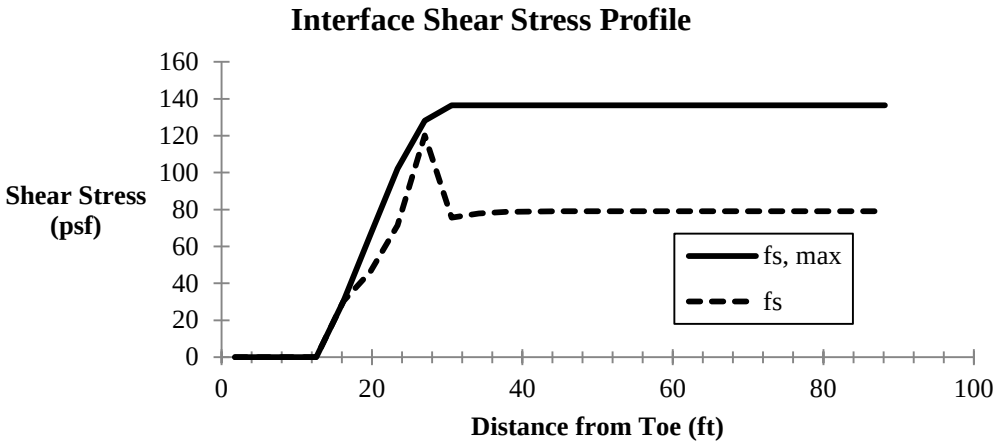

Figure 5.31: Interface shear stress profile, h_{max} = 8.5’

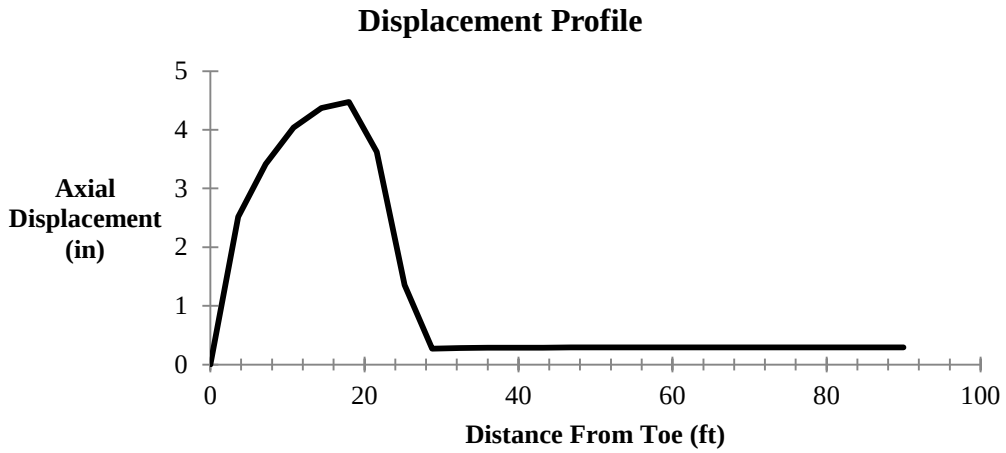

Figure 5.32: Displacement profile, h_{max} = 8.5’

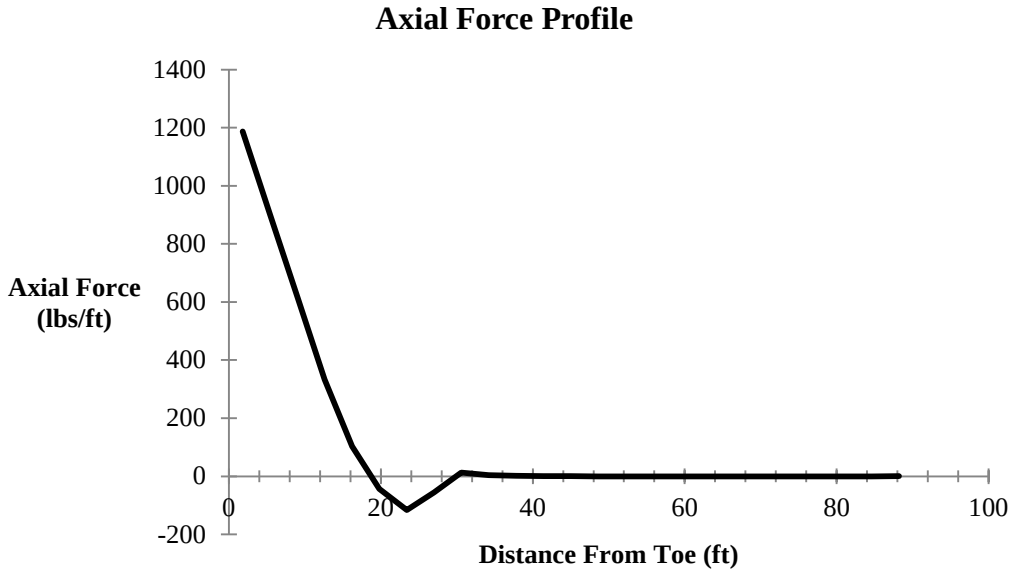

Figure 5.33: Profile of axial force per 1’ unit width of slope, h_{max} = 8.5’

5.4.3.2 Case of 67’ of geocomposite containing water, h_{max} = 21.1’

In this example, 0.7 inches of rain fall in 8 hours, and 9-ft of geocomposite drainage layer are left exposed. The constraint to flow at the drainage layer outlet is modeled with a block of soil 3 inches thick and 12 inches long, having the hydraulic conductivity of silty sand, $4*10^{-5}$ in/s ($1*10^{-4}$ cm/s). The pore pressure profile in Figure

5.35 is calculated when the water reaches its maximum elevation of 21.1 ft, which is slightly less than the equilibrium water elevation of 21.2 ft. At the maximum elevation of 21.1 ft, water fills a 67 ft length of the geocomposite drainage layer in the slope.

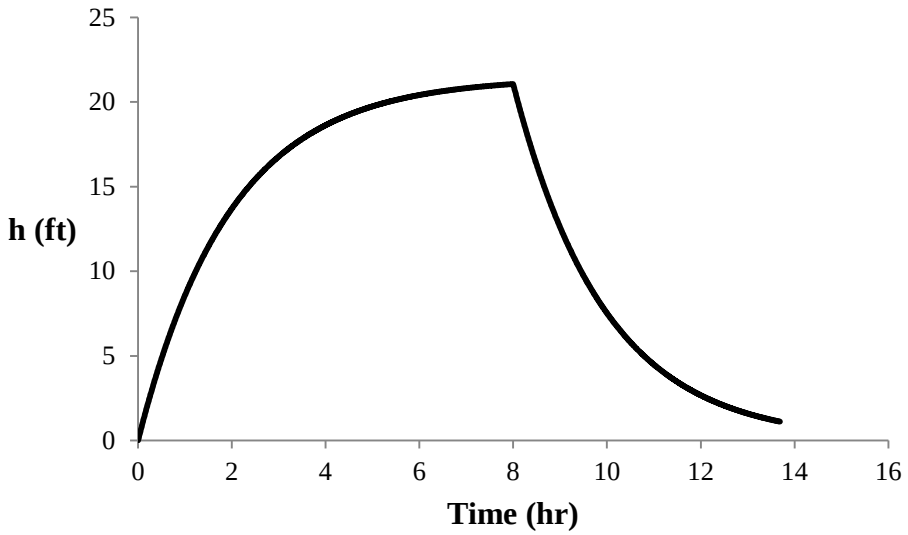

Figure 5.34: Change in water elevation in geocomposite during rain event, h_{max} = 21.1'

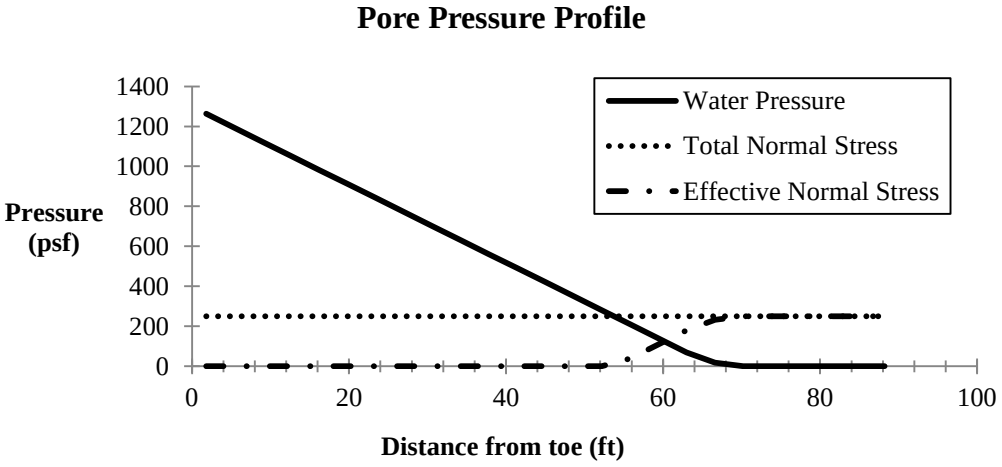

Figure 5.35: Pore pressure profile, h_{max} = 21.1'

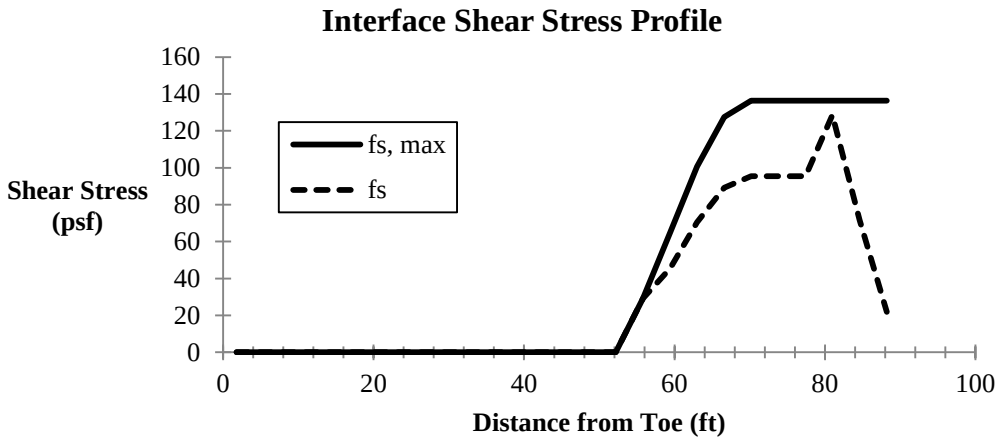

Figure 5.36: Interface shear stress profile, h_{max} = 21.1'

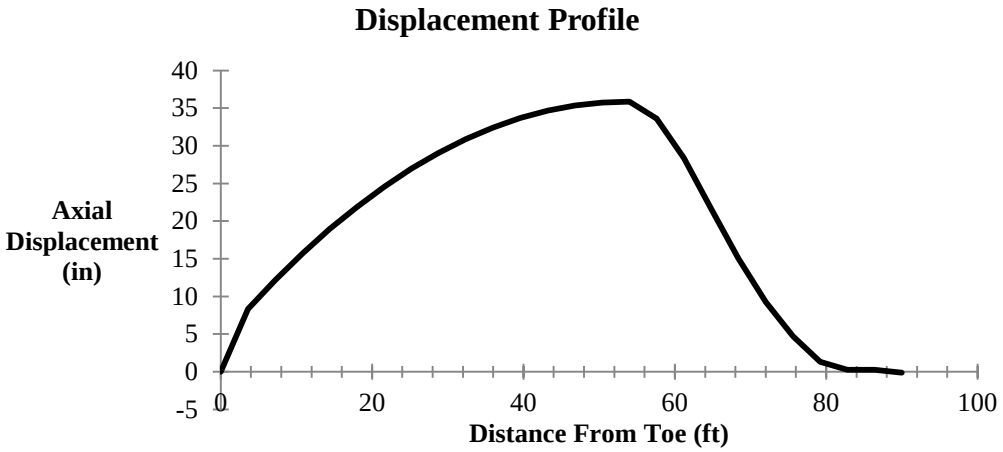

Figure 5.37: Displacement profile, h_{max} = 21.1'

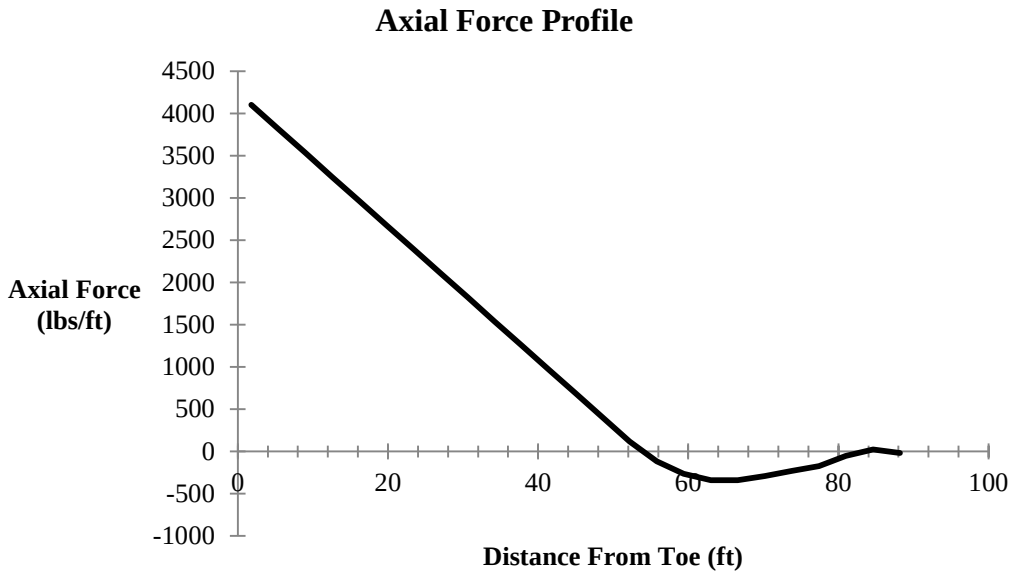

Figure 5.38: Profile of axial force per 1' unit width of slope, h_{max} = 21.1'

5.5 DISCUSSION

The example solutions demonstrate that deflections and axial compressive and tensile forces in the protective soil layer and geocomposite drainage layer generally increase as the effective stresses at the geocomposite/geomembrane interface decrease. This is an intuitive result. As pore water pressures in the geocomposite drainage layer increase, the effective stress, and therefore the available strength, along the geocomposite/geomembrane interface decreases. With less shear strength available at the interface, less of the force required to keep the slope stable comes from shear at the geocomposite/geomembrane interface, and more force must be carried axially by the "composite column" of soil and geocomposite.

Several of the example solutions showed the geocomposite drainage material in tension. In the cases of 100 psf and 200 psf uniform water pressure in the drainage layer, the geocomposite drainage material was in tension at the crest of the slope. In cases

where pore water pressures were greatest at the toe and varied along the length of the slope, the drainage material was in tension at intermediate locations along the length of the slope.

Tension in the geocomposite of any magnitude, at any location along the slope, is cause for concern. This is because geocomposite drainage layers are not designed to take tension, as they are expected to be held in place on the slope by the shear force at the interface with the underlying textured geomembrane. Panels of geocomposite drainage material are connected nominally with one tie every foot, and panel connections may be located at any elevation along the slope. Panel connections are used to hold the drainage material in place during construction, but they are not intended as structural elements of the system. Significant stability problems are expected if the drainage layer goes into tension at a panel connection.

Also consider that the stability solutions presented in this chapter are for a specific moment in time, but that in order to remain intact throughout an entire rainfall event, the slope must be stable at *every* moment in time. To be more specific, Figure 5.39 shows the geocomposite drainage layer in tension at a distance ranging from 55 ft to 85 ft from the toe of the slope. However, earlier in the rain event, before the water in the drainage layer reached its maximum elevation, lower sections of the drainage layer would have been in tension, as in Figure 5.34, where the drainage material was in tension between 20 ft and 30 ft up the slope from the toe. It is likely that a panel connection would be in tension at some time during a rain event if the water in the geocomposite exceeds the elevation of a connection at any point during the rain event, because the location of tension in the drainage material changes as water enters and exits the cover system, but the locations of the panel connections do not change.

CHAPTER 6: CONCLUSIONS AND RECOMMENDATIONS

RCRA Subtitle D notes that, "water pore pressures developed along interfaces also can dramatically reduce stability. If the design slope is steeper than the effective friction angles between the material, sliding instability generally will occur" (40 CFR 258.60(b), 6.3.3). However, a lack of requirements or design guidelines for drainage layer outlets in RCRA Subtitle D regulation makes water pressures along interfaces, and therefore sliding failures, more likely to occur.

6.1 CONCLUSIONS

The cumulative effect of prescriptive design regulation is final cover systems at new MSW landfills that are substantially similar to one another and include a geosynthetic drainage layer in contact with a textured geomembrane. However, drainage layer outlet designs vary greatly because design guidelines are not provided in the regulation. Inadequate design of the outlet could lead to clogging or other constraints to flow at the drainage layer outlet.

A model for confined flow in cover drainage systems with a constrained outlet was developed. The model is based on Darcy's Law and uses numerical methods to estimate pore water pressures in a geosynthetic drainage layer for various inflow conditions and constraints to flow at the toe outlet. Model calculations suggest that even modest constraints to flow at the drainage layer outlet have significant adverse effects on the drainage layer's ability to convey water out of the cover slope.

The strain-softening behavior of the geocomposite drainage material/textured geomemebrane interface examined depended on the effective normal stress at which the materials were displaced. Less strain-softening occurred at lower normal stresses, and more strain softening occurred at higher normal stresses. The available shear strength of

previously sheared materials depended on the strain-softening the materials has already experienced, but not on the effective normal stress at which they were re-tested.

A slope stability model was developed that satisfies force equilibrium and strain compatibility, accounts for normal stress dependent strain softerning of geosynthetic interfaces, and analyzes slopes for a variety of pore water pressure conditions, including pore pressures that may occur due to a constraint at the drainage layer outlet. In order for the cover slope to be at equilibrium, the geocomposite drainage material may be in tension at the crest of the slope or at in intermediate location, depending on the water pressure in the drainage layer.

6.2 Recommendations for Future Research

- More extensive experimental testing to further investigate the normal stress dependent strain softening behavior of geosynthetic interfaces. Only one combination of geosynthetic materials was evaluated for this research project, and only low normal stresses were tested because of the focus on landfill cover systems. More geosynthetic materials could be tested over a greater range of normal stresses to determine if conclusions reached in this study are true in general, or if they are specific to the materials tested.
- Include the concepts of effective normal stress dependent strain softening of geosynthetic interfaces and pore water pressures resulting from confined flow to more complex models of landfill cover slope stability that allow deformation and displacement of each layer of the cover system.

References

Biggs & Mathews Environmental. (2009). Final Cover Details, IESI East Texas Regional Landfill, Permit Amendment Application. Biggs & Mathews Environmental, Arlington, TX.

Ohio EPA. (2000). Final Covers for Hazardous Waste Surface Impoundments, Waste Piles, and Landfills: A Guidance Document on Requirements, Applicability, and Design. Columbus, OH.

Geosyntec Consultants. (2006). Final Cover System Details, Mesquite Creek Landfill. File 3435 – 040. Geosyntec Consultants, Austin, TX.

Gilbert, R.B. and Byrne, R.J. (1996). Strain-Softening Behavior of Waste Containment Interfaces. *Geosynthetics International*, Vol. 3, No. 2, pp. 181-203.

Gilbert, R.B., et al. (1995). A Double Shear Test Method for Measuring Interface Strength. *Proceedings of Geosynthetics '95*, IFAI, Vol. 3, Nashville, TN, February 1995, pp. 1017 – 1029.

Giroud, J.P., Zhao, A., and Bonaparte, R. (2000). The Myth of Hydraulic Transmissivity Equivalency Between Geosynthetic and Granular Liquid Collection Layers. *Geosynthetics International*, Special Issue on Liquid Collection Systems, Vol. 7, Nos. 4-6, pp. 381-401.

Golder Associates. (2001). Permit Modification for Landfill Expansion, Seabreeze Environmental Landfill, Brazora County, TX. Job #003-4501.0002. Golder Associates, Houston, TX

Koerner, R.M., and Soong, T.-Y. (2005). Analysis and Design of veneer cover soils. Geosynthetics International, Vol. 12, No. 1, pp. 28 – 49.

Li, M. H., (1995). Strength of Textured Geomembrane and Nonwoven Geotextile Interfaces. M.Sc. Thesis, The University of Texas at Austin, Austin, TX.

Liu, Chia-Nan, (1998). Reliability Analysis of Landfill Cover Slopes. PhD Dissertation, The University of Texas at Austin, Austin, TX.

Long, James, Daly, James, and Gilbert, Robert. (1993). Structural Integrity of Geosynthetic Lining and Cover Systems for Solid Waste Landfills. University of Illinois Center for Solid Waste Management and Research, Urbana, IL.

Soong, Te-Yang, and Koerner, Robert. (1996). Seepage Induced Slope Instability. *Geotextiles and Geomembranes*, Vol. 14, pp. 425-445.

U.S. EPA. (1991). Seminar Publication: Design and Construction of RCRA/CERCLA Final Covers. Washington, DC, EPA/625/4-91/025.

U.S. EPA. (1989). Technical Guidance Document: Final Covers on Hazardous Waste Landfills and Surface Impoundments. Washington, DC, EPA 530-SW-89-047.

Weaver Boos Consultants. (2005). Final Cover Details, Blue Ridge Landfill, Fort Bend County, TX. File 0120-405-11. Weaver Boos Consultants, Fort Worth, TX.

Vita

Trevor Yates was born and raised in Jamestown, Rhode Island. He graduated from high school as valedictorian of Mercersburg Academy's class of 2000 and went on to attend Duke University. As an undergraduate at Duke, Trevor double majored in Civil Engineering and Economics, was a member of the Kappa Sigma fraternity, and was captain of the varsity men's swim team. Trevor graduated with distinction from Duke in May, 2004 and moved to Chicago, where he pursued a career in the financial services industry. In August, 2009, Trevor entered the Cockrell School of Engineering at the University of Texas at Austin to pursue a graduate degree in geotechnical engineering.

Email: tbyates@gmail.com

This thesis was typed by the author.